NASA CR-72399

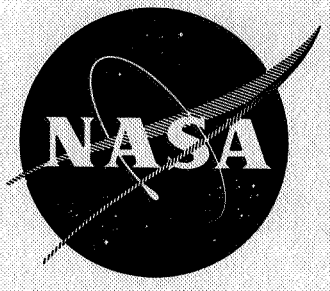

An Experimental Investigation of Near Critical and Supercritical Burning of Bipropellant Droplets

by

D. P. Dominicis

prepared for

NATIONAL AERONAUTICS AND SPACE ADMINISTRATION
CONTRACT NGR 39-009-077

Mechanical Engineering Department
The Pennsylvania State University
University Park, Pa.

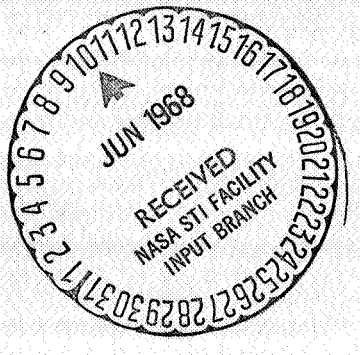

NASA CR-72399

AN EXPERIMENTAL INVESTIGATION OF NEAR CRITICAL AND SUPERCRITICAL BURNING OF BIPROPELLANT DROPLETS

by

D. P. Dominicis

prepared for

National Aeronautics and Space Administration

April 10, 1968

Contract: NGR 39-009-077

Technical Management
NASA Lewis Research Center
Cleveland, Ohio
Chemistry and Energy Conversion Division
Paul R. Wieber

Mechanical Engineering Department
The Pennsylvania State University
University Park, Pa.

AN EXPERIMENTAL INVESTIGATION OF NEAR CRITICAL AND SUPERCRITICAL BURNING OF BIPROPELLANT DROPLETS

by

D. P. Dominicis

ABSTRACT

This report presents the results of an investigation of droplet combustion in air at pressures sufficiently high for the droplet to exceed its critical temperature during combustion. For the tests, the droplet was supported from a quartz fiber or a thermocouple, contained within a small pressurized chamber. To prevent the droplet from falling from its support due to reduced surface tension, the experiment was carried out under zero-gravity conditions. Combustion lifetimes and droplet temperature measurements are reported over a pressure range from 100 to 2000 psia for n-decane and n-hexadecane. Experimental supercritical burning times were found to agree reasonably well with available theoretical predictions.

TABLE OF CONTENTS

LIST OF TABLES

LIST OF FIGURES

Figure | Page

NOMENCLATURE

A	Area (FT^2)
A_ℓ	Surface Area of Droplet (FT^2)
A_w	Cross Sectional Area of Thermocouple Wire (FT^2)
a	Apparent Droplet Radius (FT)
B_k	Constant in the Frequency Factor for the kth Reaction
D	Diffusion Coefficient (FT^2/SEC)
D_{ij}	Binary Diffusion Coefficient for Species i and j (CM^2/SEC)
D_p	Spherical Particle Diameter (FT)
d	Droplet Diameter (FT)
E_k	Activation Energy for the kth Reaction (BTU/MOLE)
h	Convection Heat Transfer Coefficient (BTU/HR FT^2 °R)
k_f	Thermal Conductivity of Droplet Fluid (BTU/HR FT °R)
k_g	Thermal Conductivity of Gas Around Droplet (BTU/HR FT °R)
k_w	Thermal Conductivity of Thermocouple Wire (BTU/HR FT °R)
ℓ_1	Minor Ellipse Axis (FT)
ℓ_2	Major Ellipse Axis (FT)
M	Molecular Weight
Nu	Dimensionless Nusselt Number
P	Pressure (ATM)
P_{cr}	Critical Pressure (ATM)
q_f	Heat Transfer Rate Through Surrounding Gas (BTU/HR FT^2)
q_w	Heat Transfer Rate Through Thermocouple Wires (BTU/HR FT^2)

r	Radial Coordinate (FT)
r_f	Flame Radius (FT)
r_ℓ	Droplet Radius (FT)
$R°$	Universal Gas Constant (BTU/Mole °R)
t	Time (SEC)
t_b	Burning Time (SEC)
t_c	Corrected Time (SEC)
t_m	Measured Time (SEC)
T	Temperature (°R)
T_{cr}	Critical Temperature (°K)
T_f	Flame Temperature (°R)
T_ℓ	Droplet Temperature (°R)
$\vec{V}$	Mass Average Velocity of Gas Mixture (FT/SEC)
$\vec{V}_i$	Diffusion Velocity of Species i (FT/SEC)
W_f	Injected Droplet Mass (LB_M)
W_i	Molecular Weight of Species i
W_{in}	Initial Mass of Fuel in the System (LB_M)
W_t	Total Mass of Fuel in the System (LB_M)
W_F	Molecular Weight of Fuel
W_0	Molecular Weight of Oxidant
W_P	Molecular Weight of Products
w_i	Rate of Production of Species i by Chemical Reactions (LB_M/FT^3 SEC)
X_i	Mole Fraction of Species i
$Y_{F,\ell}$	Mass Fraction of Fuel at the Droplet Surface
Y_i	Mass Fraction of Species i

$Y_{0\infty}$	Mass Fraction of Oxidant Far From the Droplet
$Y_{P\infty}$	Mass Fraction of Products Far From the Droplet
α_i	Dimensionless Variable, $Y_i/W_i(\nu_i'' - \nu_i')$
α_k	Exponent Determining Temperature Dependence of the Frequency Factor for the kth Reaction
β'	Dimensionless Variable $\alpha_P - \alpha_F$
Γ	Dimensionless Variable $(\beta' - \beta_\infty')/(\beta_0' - \beta_\infty')$
η	Dimensionless Radius (r/a)
η_f	Dimensionless Flame Radius (r_f/a)
θ	Dimensionless Time $4\pi Dt/(W_f/\rho\Gamma)^{2/3}$
ν	Stoichiometry Parameter $(Y_{0\infty}/Y_{F,\ell})/\nu_0 W_0/\nu_F W_F)$
$\nu_{i,k}'$	Stoichiometric Coefficient for Species i Appearing as a Reactant in Reaction k
$\nu_{i,k}''$	Stoichiometric Coefficient for Species i Appearing as a Product in Reaction k
ν_F	Stoichiometric Coefficient for Fuel
ν_0	Stoichiometric Coefficient for Oxidant
ν_P	Stoichiometric Coefficient for Products
ρ	Average Density (LB_M/FT^3)
ρ_ℓ	Liquid Droplet Density (LB_M/FT^3)
σ_{12}	Leonard Jones Force Constant (Å)
τ	Dimensionless Time $(t\ D_{12}/a^2)$
τ_b	Dimensionless Burning Time $(t_b\ D_{12}/a^2)$
τ'	Particle Time Constant (SEC)
τ_D'	Droplet Time Constant in Surrounding Gas (SEC)
τ_{tc}'	Thermocouple Time Constant (SEC)

ϕ	Dimensionless Flame Radius $r_f/(W_f/\rho\Gamma)^{1/3}$
Ω_d	Collision Integral
ω	Reaction Rate (MOLES/FT^3 SEC)

CHAPTER 1

INTRODUCTION

1.1 General Statement of the Problem

Fuels for propulsion and power systems can be categorized as being either bipropellants or monopropellants. A bipropellant fuel system consists of separate fuel and oxidizer streams which are combined and burned within a combustion chamber. In a monopropellant system a single stream of propellant is decomposed in the combustion chamber to form high temperature gaseous products.

Due to the widespread use of bipropellants, numerous investigations have been undertaken in recent years with the overall objective of developing methods for predicting bipropellant combustion chamber performance. An integral part of this work is a good understanding of the combustion characteristics of individual fuel droplets. The present investigation is a contribution to this aspect of the bipropellant combustion problem with particular emphasis on the high pressure combustion characteristics of single fuel droplets burning in air.

1.2 Previous Work

In attempting to predict combustor performance, Priem (1) developed a model using droplet vaporization as the rate controlling

process in a combustion chamber. Priem calculated the effect of drop size, initial drop velocity, final gas velocity, chamber pressure, initial liquid temperature and gas temperature on the chamber length necessary to complete the vaporization of a singlet droplet. Priem and Heidmann (2) modified Priem's original analysis and used it to model bipropellant spray characteristics. Their predictions were correlated with actual combustor performance and were found to agree well at moderate pressures. The importance of Priem and Heidmann's work is in the fact that they used a model based on individual droplet characteristics to predict combustor performance. This approach has been widely employed in design applications.

The success of the Priem and Heidmann model pointed out the necessity of understanding the combustion of individual fuel droplets. The earliest studies of single droplet combustion centered on the "steady burning period." This is the portion of the droplet's burning lifetime where all the heat transferred to the droplet from the flame is utilized for the heat of vaporization of the fuel leaving the droplet surface. During steady burning the temperature of the droplet remains constant at its so-called "wet bulb" temperature, which is slightly below the boiling temperature of the fuel at the ambient pressure. Various predictions of the burning rate have resulted from analysis of the steady burning period (3-5), and they were found to generally agree with experimental results at atmospheric pressure (4-7).

Investigators at the University of Wisconsin modified the earlier analysis by considering as well the heating of the droplet

from its initial temperature to the wet bulb temperature (8-10). The Wisconsin studies considered vaporization during heating and at the wet bulb state. The predicted life histories agreed adequately with measurements of droplets vaporizing in the absence of combustion in an air environment at temperatures up to 620°F and pressures from 1-4 atmospheres.

The studies mentioned above all approach droplet combustion by means of a quasi-steady analysis making the following assumptions:

1. The reaction takes place in the gas surrounding the droplet.
2. The temperature and concentration profiles in the gas phase adjust instantaneously to changes in droplet temperature, diameter, velocity, and droplet surface fuel concentration, i.e. the profiles are steady state profiles for the existing boundary conditions at each instant of time.
3. The radial motion of the droplet surface, due to evaporation is assumed to have a negligible influence on transport rates.
4. The reaction zone is assumed either to be thin (3-5); or sufficiently far from the droplet so that it exerts a negligible influence on transport rates (1, 2).
5. Fuel is consumed in the reaction zone at the same rate as it evaporates from the droplet.

The assumptions of the quasi-steady analysis become questionable at high ambient pressure. This was pointed out by Williams (11) and Brzustowski (12), who attempted to set limits on the range of validity of the quasi-steady analysis.

If the droplet radius regression rate is assumed to be negligible compared to the velocity of the vapor leaving the liquid surface, this implies that the liquid density is much greater than the vapor density. This is no longer true at high pressures. In addition, at elevated pressures, the ability of the concentration and thermal boundary layers around the droplet to adjust rapidly enough to maintain steady state profiles, as required by the quasi-steady theories, becomes questionable.

Another aspect of the high pressure combustion problem was considered by Wieber (13). This is the possibility that the droplet may reach its critical temperature before the end of combustion. Wieber used a quasi-steady analysis to calculate a droplet's approach to the critical point. Performing calculations on an n-heptane droplet, he found that for pressures of two to three times the critical pressure, very little of the initial mass of the droplet had vaporized before the droplet reached its critical temperature. Wieber indicated that supercritical burning could be encountered in high pressure systems such as rocket and diesel engines.

Spalding (14) described a model for supercritical combustion. At the critical point the droplet has essentially become a pocket of gas. Spalding approximated the vapor pocket as a point source of fuel. The combustion process was presented by the flame surface

approximation, i.e. a diffusion controlled flame with an infinitely thin reaction zone. Thus, considerations of chemical kinetics were eliminated. Rosner (15) has modified Spalding's analysis by considering the fuel vapor pocket to be of finite dimensions. The following additional assumptions were made by Spalding and Rosner:

1. A single, irreversible reaction occurs in the flame zone.
2. Fuel and oxidizer diffusion are described by a pseudo-binary Fick's diffusion law with equal diffusion coefficients.
3. Reactant transport by convection is negligible compared with diffusion.
4. Fluid properties are constant.

The analyses by Spalding and Rosner are applicable to a droplet burning above the critical point. Both theories predict a pressure dependence of one third and an initial diameter squared dependence for the droplet burning lifetimes. These predictions have not been verified experimentally. A detailed derivation of the Spalding and Rosner theories is found in Appendix A.

Experimental investigations of single droplet combustion have most often been conducted on suspended droplets (4-10). Hall and Diederichsen (16) have conducted suspended droplet experiments at elevated pressures, measuring droplet burning lifetimes after ignition as a function of pressure and initial drop diameter. Their work considered pressures as high as twenty atmospheres but they were unable to extend into the near critical and supercritical

combustion regime. In these experiments, at pressures near the critical pressure, the droplet fell from its support due to the reduction in surface tension near the critical point.

Recently Brzustowski and Natarajan (17) observed the combustion of aniline droplets at pressures as high as 814 psia, 44 psi above the critical pressure of aniline. In this experiment the droplet did not fall from its support, indicating that the near critical burning regime was not reached. This result would be expected from Wieber's (13) prediction; that the pressure must be two to three times the critical pressure for appreciable amounts of the fuel to remain when the critical temperature is reached for fuels of this type. Brzustowski and Natarajan measured burning rate constants of aniline at pressures below 200 psi, and burning lifetimes at higher pressures. Difficulty in obtaining clear silhouette photographs above 200 psi prevented measurement of the burning rate constants at high pressures.

Another experiment relevant to the present investigation was conducted by Kumagai and Isoda (18). They observed the combustion of individual suspended droplets at atmospheric pressure in a chamber subjected to various gravity fields in order to observe the effect of natural convection. They found that the flame shape is spherical in free fall (zero gravity) but changes considerably under weak gravity fields. Also, the droplet's burning rate decreases as gravitational acceleration decreases, since the flame moves further from the droplet due to the reduction of natural convection effects.

1.3 Specific Statement of the Problem

The preceding discussion illustrates the need for experimental work on high pressure droplet burning. Here the quasi-steady theory is questionable and the high pressure combustion models have not been verified. With this in mind the present investigation was undertaken with the following objectives:

1. To examine experimentally the combustion of individual, supported, bipropellant droplets under pressures which would produce near critical and supercritical burning.
2. To compare the existing quasi-steady and high pressure combustion theories with the experimental results, and make any modifications necessary to obtain reliable predictions for droplet life histories.

The preliminary stage of the investigation, discussed in this paper, consisted of developing an apparatus capable of carrying out the experimental objective. In addition, preliminary experiments were conducted in the near critical and supercritical burning regime.

It was mentioned previously that the droplet tends to fall from its support near the critical point. To avoid this, the experiment was carried out in zero gravity by means of a free fall apparatus. The zero gravity facility additionally eliminated natural convection, thus permitting the experiment to more closely represent the theoretical models.

The fuels used in the study were n-decane and n-hexadecane. They were burned in air at room temperature and pressures ranging from 14.2 to 2000 psia.

CHAPTER 2

APPARATUS

2.1 Test Facility

The requirements for the experimental apparatus were to provide an environment at high pressure (up to 2000 psia) where a droplet can be ignited and burned under zero gravity conditions. It was also necessary to provide a means of observing combustion and measuring the temperature variation of the droplet.

The high pressure droplet reaction chamber is shown in Figure 1. Figure 2 is a photograph of the chamber. The reaction chamber was constructed of stainless steel and was cylindrical in shape. The chamber was 4 in. long and 2 7/8 in. in diameter. The chamber could be opened at one end by means of a removable stainless steel end plate which was secured to the droplet chamber by a large flange on the end of the chamber. An "O" ring was installed between the end plate and the flange to permit sealing. The end plate and chamber were held together by six 1/2 in. stainless steel bolts. A small quartz window was built into the end plate and a first surfaced mirror was mounted on the end plate to permit photographing the combustion process. The closed end of the reaction chamber was also provided with a quartz window for background lighting and visual observation of the droplet. A removable plug in the wall of the

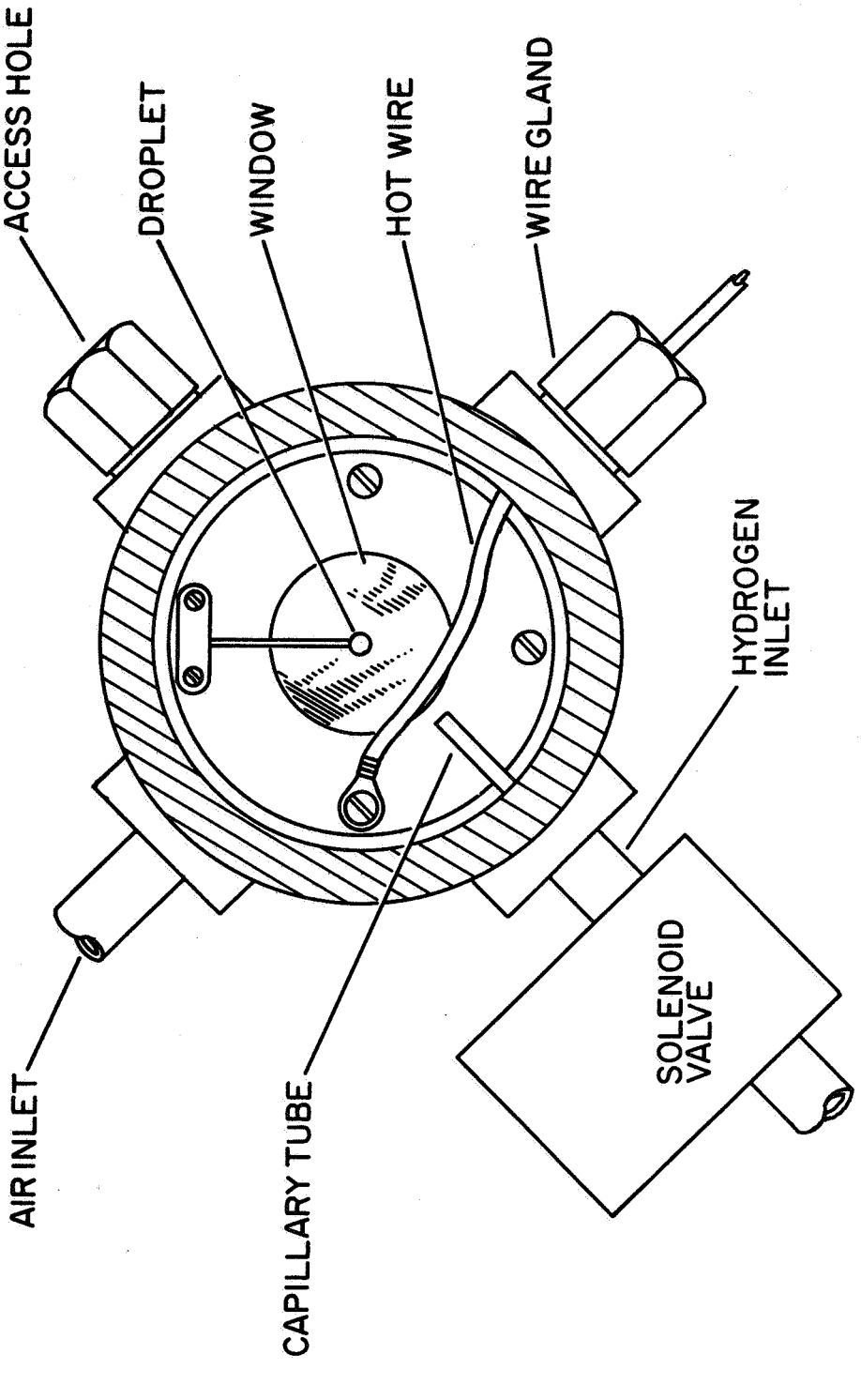

FIG. 1 SKETCH OF THE DROPLET CHAMBER

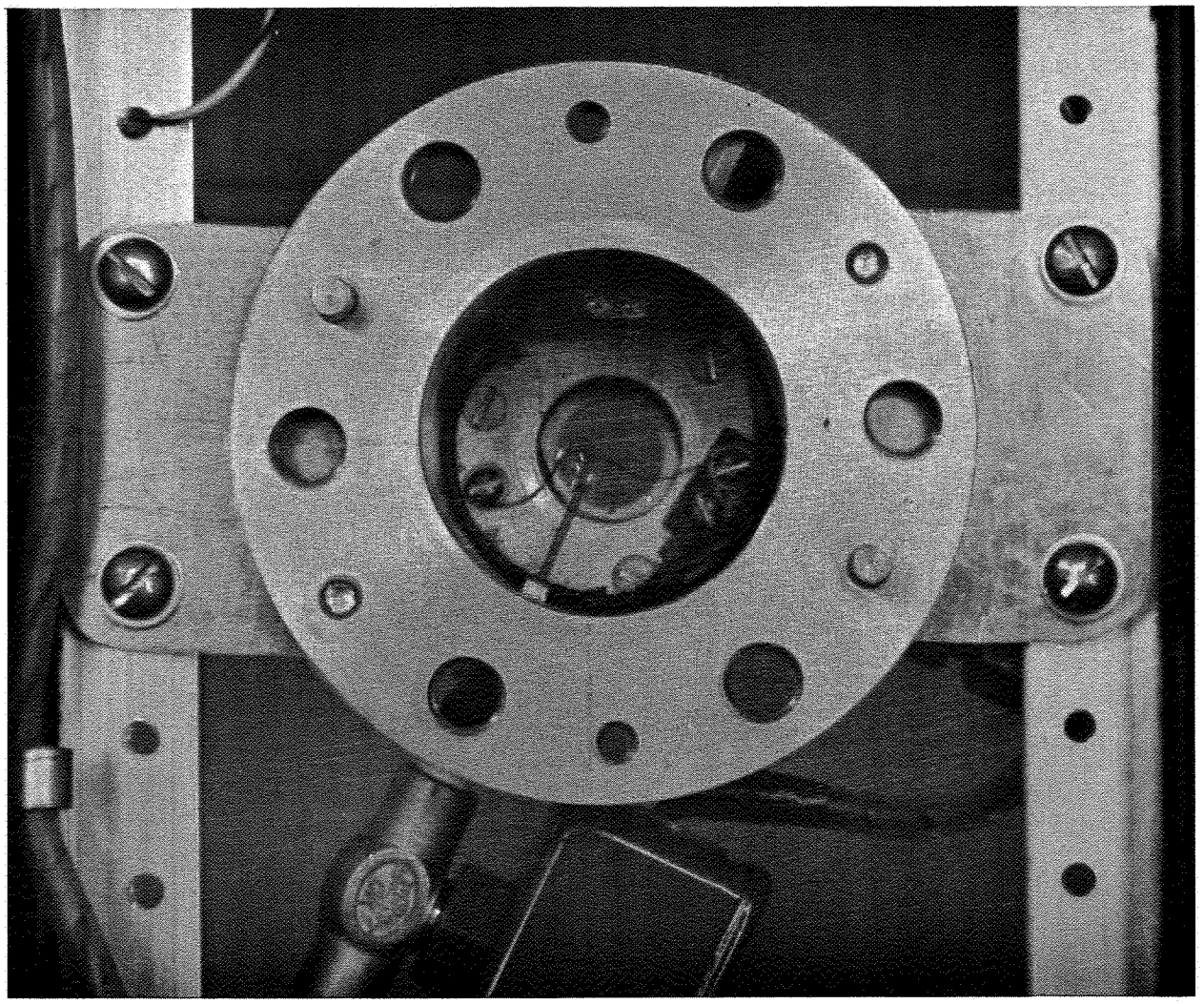

FIG. 2 PHOTOGRAPH OF THE DROPLET CHAMBER

chamber allowed the droplet to be mounted on its support by a hypodermic needle. Electrical connections into the high pressure chamber were provided by a Conax 4 wire gland. The droplet chamber was hydrostatically tested to 2300 psi.

The droplet was mounted on either a quartz fiber or on the junction of a chromel-alumel thermocouple as shown in Figure 1. The thermocouple permitted measurement of the droplet temperature during burning. The quartz fiber was approximately 0.008 in. in diameter with a 0.014 in. diameter bead at the end. The thermocouple wires were 0.003 in. in diameter with a junction approximately 0.009 in. in diameter. With these dimensions, the time constant of the droplet in the high temperature gas, following ignition is roughly 11 times longer than the time constant of the thermocouple in the droplet liquid (see Appendix B). On this basis, it was assumed that the thermocouple gave an adequate representation of the temperature variation of the droplet.

Two different methods for igniting the droplet were employed. The first consisted of directing a hydrogen diffusion flame toward the droplet until it ignited. The hydrogen flame was extinguished as soon as possible after ignition, since the presence of gas flow caused a disturbance to the droplet, especially at higher pressures.

The hydrogen was stored in a small tank mounted inside the free fall apparatus (Figure 3). The pressure in the storage tank was kept slightly higher than that of the droplet reaction chamber. The storage tank was used to increase the capacity of the hydrogen system, so that the hydrogen flow into the droplet chamber was

uniform during a test. The flow of hydrogen into the droplet chamber was controlled by a solenoid valve which was automatically actuated at the beginning of the free fall period. The hydrogen was introduced into the droplet chamber through a capillary tube mounted in the chamber wall as shown in Figure 1. An electrically heated wire ignited the entering hydrogen, which in turn ignited the droplet. This scheme was also used by Hall and Diederichsen (16) with a bench mounted apparatus.

The flame ignitor system did not operate well at high pressures. The hydrogen solenoid became hard to control and the hydrogen flow caused a great deal of disturbance to the droplet, often shearing it apart or knocking it from its mount. Due to this problem, another ignition method was tried.

The second ignition method employed the hot wire to directly ignite the droplet. This was accomplished by moving the wire in closer to the droplet and eliminating the hydrogen system. At the beginning of the free fall period, electrical power was supplied to the wire, causing it to heat up and ignite the droplet. This method was superior to the flame ignitor method in that it provided a more reliable ignition with much less disturbance to the droplet.

The free fall chamber is shown in Figure 3, with a photograph of the free fall apparatus shown in Figure 4. It consisted of an aluminum shell 8 3/4 in. in diameter and 32 in. long with two doors along its length to provide easy access to the internal components. The free fall chamber was hung in place by a pin mechanism which automatically released at the start of a test. Release of the free

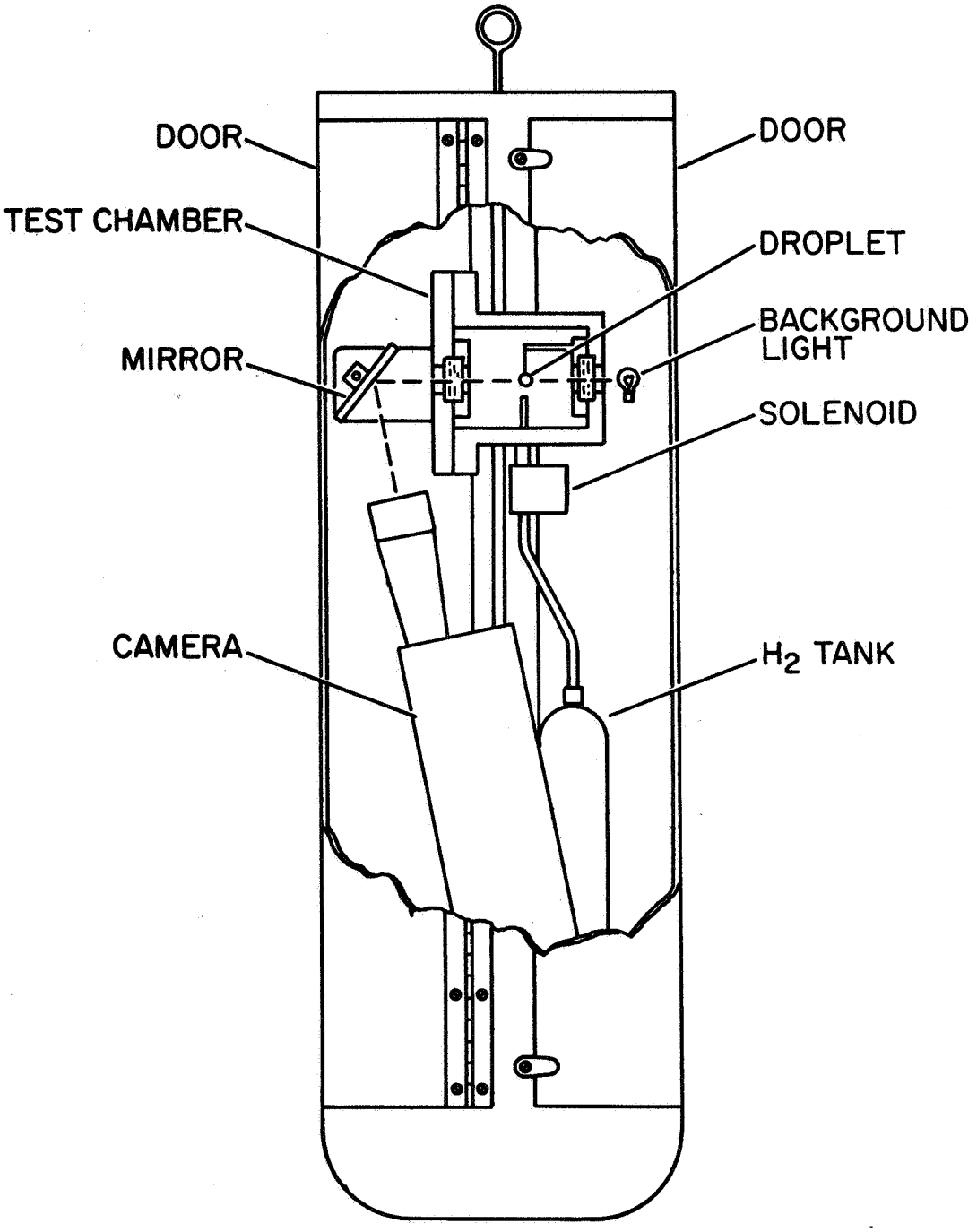

FIG. 3 SKETCH OF THE FREE FALL CHAMBER

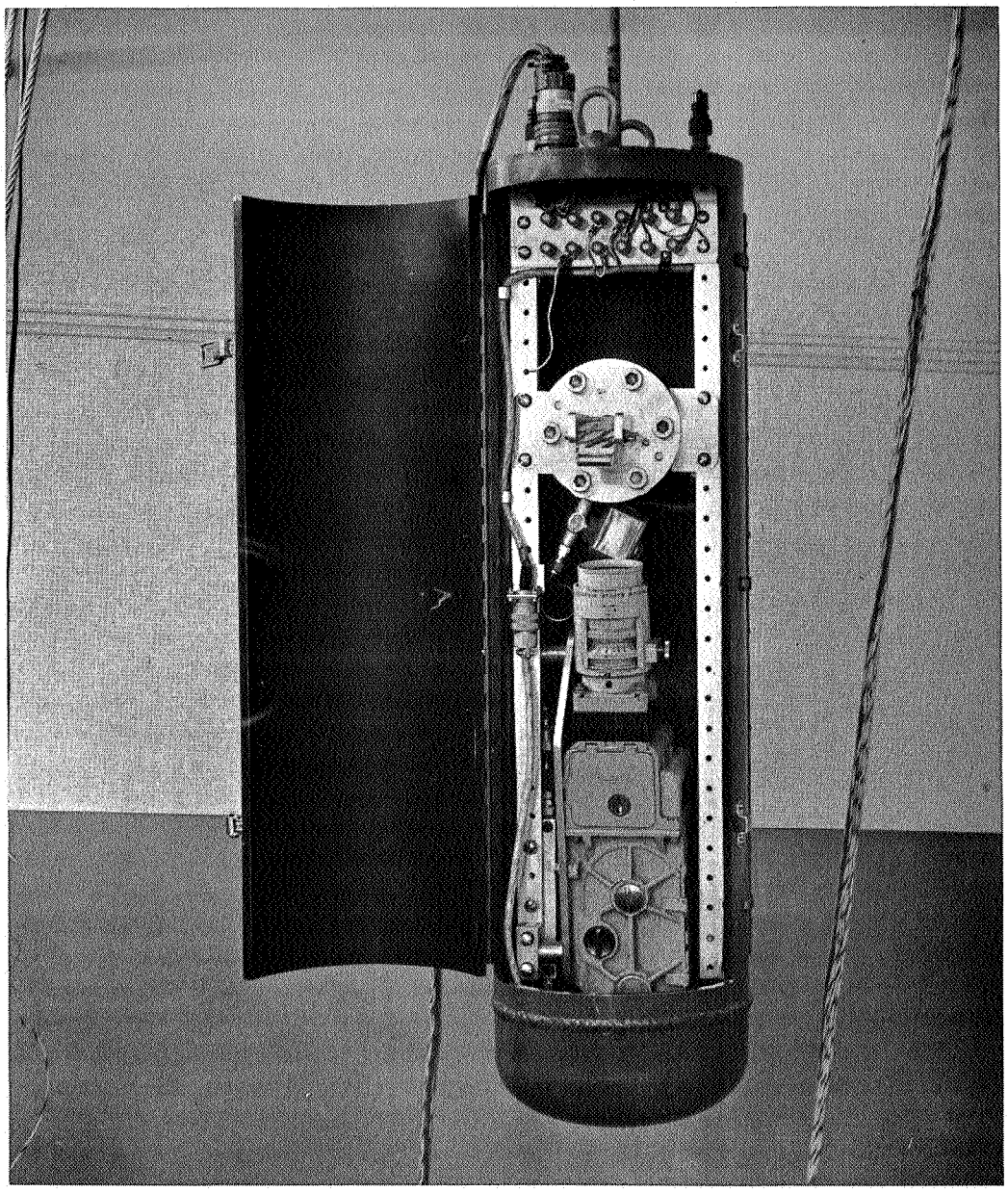

FIG. 4 PHOTOGRAPH OF THE FREE FALL CHAMBER

fall chamber was accomplished by a pneumatic cylinder which was automatically activated by a solenoid valve. The apparatus dropped approximately 16 feet into a tub of chopped Resilite, a foam plastic, which adsorbed the shock of the fall. The zero-gravity facility provided a test time of about one second.

Drag forces on the drop chamber were estimated to be negligible. For example, using a total apparatus weight of 60 lb_m and a chamber diameter of 8 in., with a drag coefficient conservatively estimated at unity, the maximum net gravity force is on the order of 0.007 g.

Referring again to Figure 3, the background light employed was an NE 51 neon bulb, powered by a D.C. source to give steady illumination. The back lighting permitted a silhouette photograph of the droplet just before the beginning of a test, thus allowing a measurement of the droplet's initial size. The light was turned off soon afterward to permit dark field photographs of the ignition and combustion processes.

A Wollensak Fastair 16 mm high speed motion picture camera was employed for the droplet photographs. The camera was mounted below the reaction chamber as shown in Figure 3. The film speed during the tests was approximately 100 frames per second. The camera was equipped with an internal timing marker to allow time correlation of the films. The film used was Kodak Tri-X Negative emulsion TXN 430.

High pressure gas was provided by commercially pure dry air and hydrogen in cylinders. The gas pressures in the reaction

chamber and in the hydrogen line were measured by 0-3000 psi bourdon tube gages with 25 psi subdivisions. For pressures below 100 psi, a 0-100 psi Ashcroft laboratory test gage with 1/2 psi subdivisions was used. All gages were calibrated with a dead weight tester.

The signal from the thermocouple was fed through a CEC 1-165 D.C. amplifier to a CEC 5-124 oscillograph. The two galvanometers used were CEC type 7-317 fluid damped galvanometers with a flat, five percent frequency response to 2200 cps. One galvanometer was used to measure the thermocouple output, and the other simply deflected when the neon background light was turned off. The recorder employed an internal flash timing unit for time sequencing the chart record. The temperature trace could be synchronized with the film by the extinction of the background light. This event was recorded by the camera and by the second galvanometer and was thus used as the origin of time in tests using the thermocouple.

Two timing devices were used to provide virtually automatic operation of the apparatus. The first was a falling weight switch which consisted of a steel block which dropped through guide rods and actuated small knife blade switches along its path. The weight was held in its uppermost position by an electromagnet and released automatically. This arrangement was used for functions which required accurate time sequencing, such as the actuation of the hydrogen solenoid or the hot wire and the release of the free fall chamber. Less critical functions were controlled by a cycling timer. This device controlled the background light, electromagnet, recorder and camera.

2.2 Operation of the Apparatus

The preliminary setup of the experiment involved focusing and checking the operation of the camera, setting the air and hydrogen pressure and pressurizing the air line used to release the free fall chamber. The thermocouple output was calibrated by a Leeds and Northrup 8690 millivolt potentiometer to obtain the sensitivity of the galvanometer-amplifier circuit. In addition, the thermocouple-amplifier-galvanometer circuit was checked occasionally with a boiling water bath as a reference temperature. In tests with the hydrogen ignitor no temperature record was made. In conducting a test, the droplet was mounted on a quartz fiber or thermocouple junction and the droplet chamber was closed and pressurized. In the flame ignitor tests the hydrogen line was also pressurized at this time. The air and hydrogen hoses were removed by means of two quick-disconnect fittings at the top of the free fall chamber.

For tests with the flame ignitor it was necessary to run a preliminary "purge cycle" for the hydrogen line. The purge cycle operated through the Cramer timer which opened the hydrogen solenoid for approximately one second. This released hydrogen into the capillary tube and forced air out of the tube. More reliable ignition was obtained when this procedure was employed before each test.

After the purge cycle, the weight in the dropping weight switch was raised to its highest position and held there by the electromagnet, and the knife blade switches were set. Panel switches controlling the hot wire, background light, hydrogen solenoid, and

free fall chamber release solenoid were closed, permitting automatic control of these components by the Cramer timer and the dropping weight switch. The start switch for the Cramer timer was closed and the actual test began.

Once the timer was actuated, the sequence of events in a hydrogen flame ignitor test was as follows:

1. background light on
2. camera on
3. background light off
4. hot wire on
5. electromagnet de-energized-weight falls
6. weight trips release solenoid switch and free fall begins
7. weight closes upper hydrogen solenoid switch, solenoid valve opens, and releases hydrogen into chamber
8. hydrogen ignited by hot wire
9. hydrogen flame ignites droplet
10. dropping weight opens lower hydrogen solenoid switch, closing the solenoid and stopping the flow of hydrogen
11. all components off at the end of the free fall period.

In the hot wire ignitor test there was no purge cycle and all functions of the hydrogen system were eliminated. Control of the hot wire was transferred to the dropping weight switch. Thus the

hot wire was supplied with power only momentarily, consistent with reliable ignition. Also, the CEC recorder was operated during the same time period as the camera.

The data consisted of the motion picture film and the oscillograph record of the droplet temperature. The time of ignition of the hydrogen jet, droplet ignition and droplet burnout were found from the film. Also, the initial droplet size was obtained from the silhouette photographs.

Since the droplets were usually elliptical in shape, a diameter correction, suggested by Kobayasi (6), was used which gave an equivalent diameter for a sphere having the same volume as the elliptical droplet. The formula employed was as follows:

$$d = 3\sqrt{\ell_1 \ell_2^2} \tag{2.1}$$

The symbols are defined in the Nomenclature section.

CHAPTER 3

RESULTS OF THE FLAME IGNITOR TESTS

For the tests with the flame ignitor, the droplet was mounted on a quartz fiber and no temperature measurements were made. Figure 5 shows a typical film record at low pressure with the flame ignitor. The test shown is an n-decane droplet burning in air at a total pressure of 114 psia.

The first strip of film in Figure 5 is the silhouette photograph of the droplet. The white circular field is the background light, in this case an incandescent bulb. The droplet ignites almost immediately after contact with the hydrogen flame. The flame from the burning droplet is easily distinguished from the hydrogen flame due to its greater luminosity. It is notable that the flame is extended into a teardrop shape in this test, indicating the presence of convection. This is due to induced gas flow from the hydrogen flame, not natural convection. The droplet does not appear to leave the probe location during the test.

Figure 6 is a typical test at high pressure using the flame ignitor. The fuel was n-decane burning in air at 814 psia. Here the presence of the induced flow from the hydrogen flame caused a significant disturbance to the combustion process. Distortion and shearing of the combustion zone is evident, and the droplet appears to leave the probe location toward the end of burning.

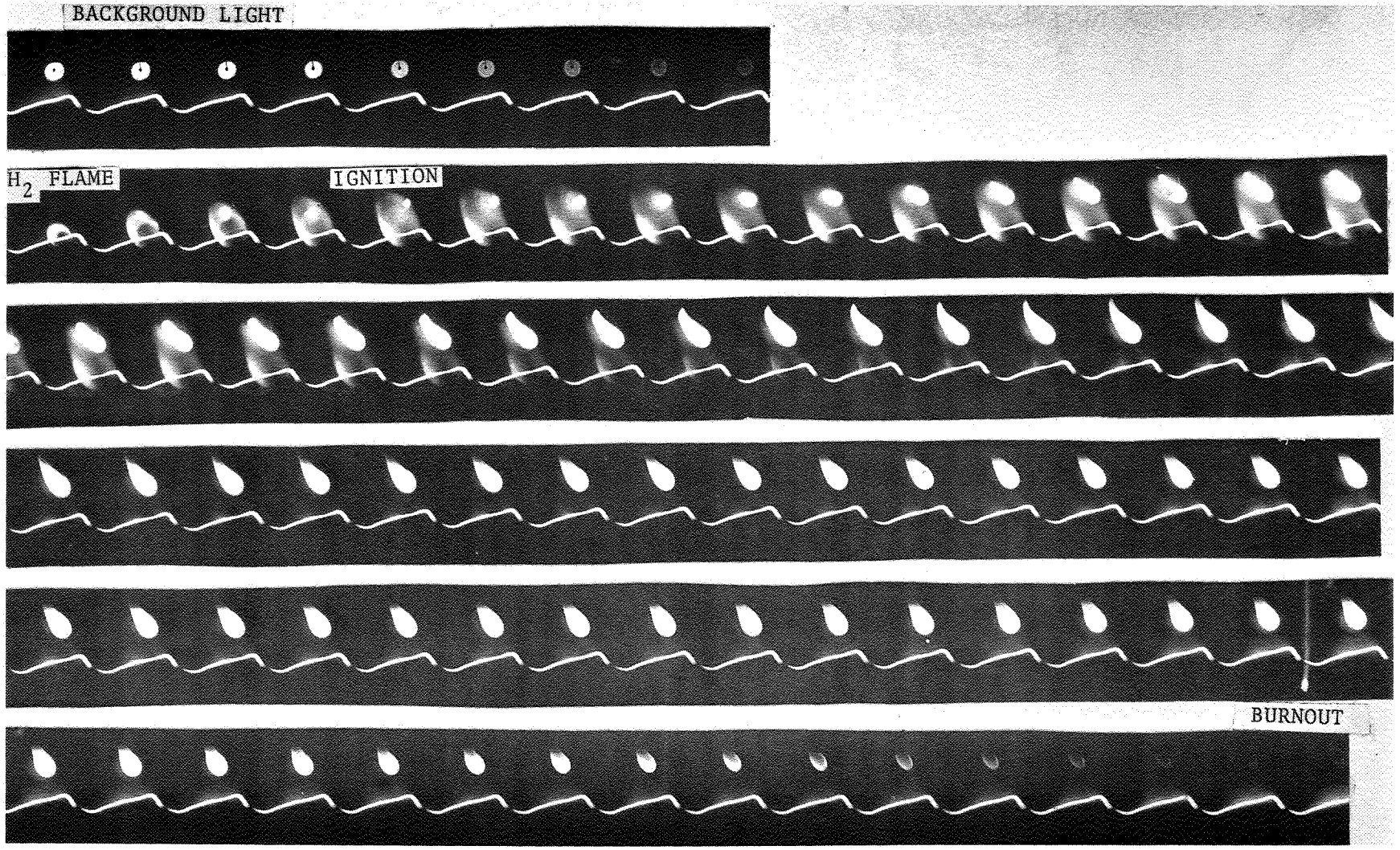

FIG. 5 COMBUSTION AT LOW PRESSURE (114 PSIA) WITH THE FLAME IGNITOR

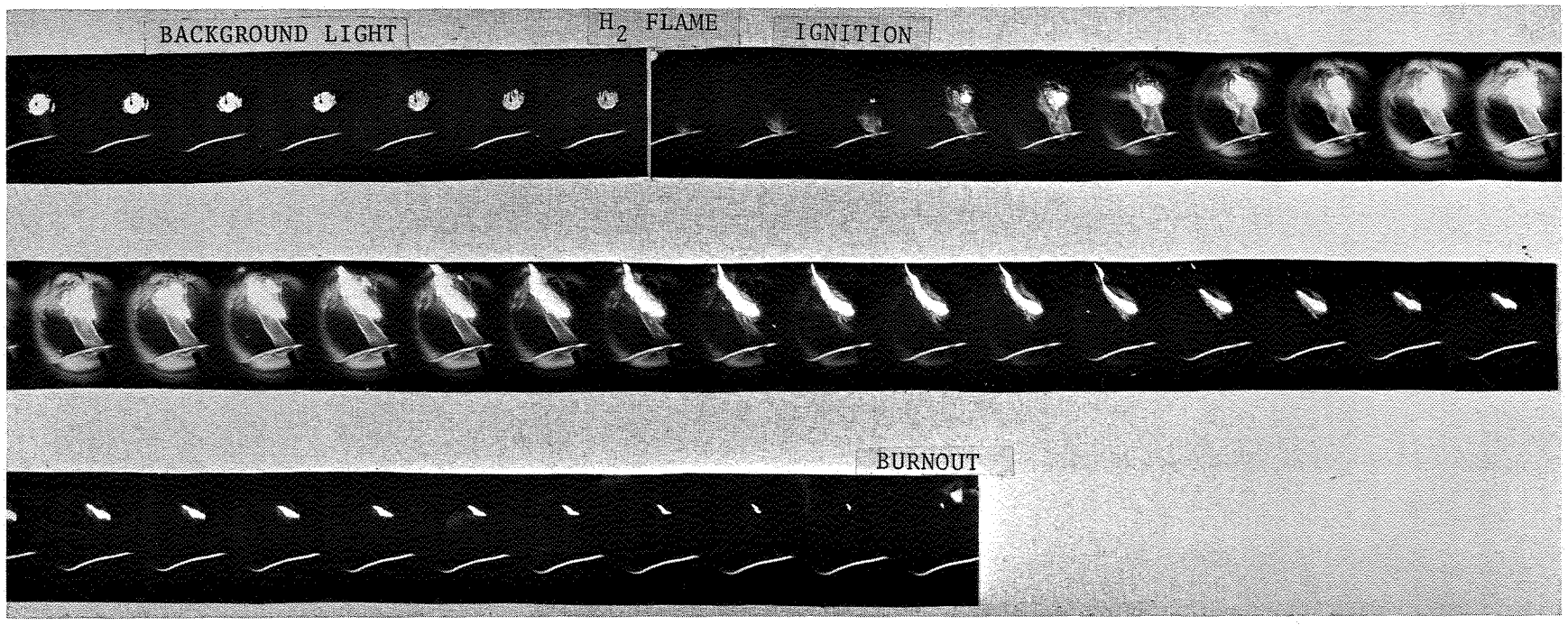

FIG. 6 COMBUSTION AT HIGH PRESSURE (814 PSIA) WITH THE FLAME IGNITOR

Measurements of the combustion lifetimes were made from the films. Combustion lifetime was defined as the time between ignition and the end of luminosity of the flame. This is the definition used by Hall and Diederichsen (16).

Figure 7 shows measured lifetimes as a function of pressure for n-decane droplets of approximately the same initial diameter (740 ± 50 μ). Data from Hall and Diederichsen (16) for the same fuel and initial droplet size is also shown on the figure. The critical pressure was obtained from Reference 19.

The data from the present investigation and from Reference 16 both show the same trend of decreasing lifetime with increasing pressure. The lifetimes are seen to be longer for the present study, and this is probably due to the elimination of natural convection by the zero gravity apparatus. Kumagai and Isoda (18) demonstrated that the flame moves in closer to the droplet in one-g, causing higher heat transfer rates and higher evaporation rates. The result is a shorter lifetime in one-g.

Figures 5 and 6 showed that there was convection in the zero-g tests due to induced flow from the flame ignitor. The magnitude of the natural convection compared to convection from induced flow was demonstrated in some one-g tests. In one-g, the hydrogen flame rose almost straight up rather than remaining in the direction of the capillary tube, as was seen in Figures 5 and 6. This indicates that the flame's upward momentum due to natural convection was much greater than the momentum in the direction of the capillary tube.

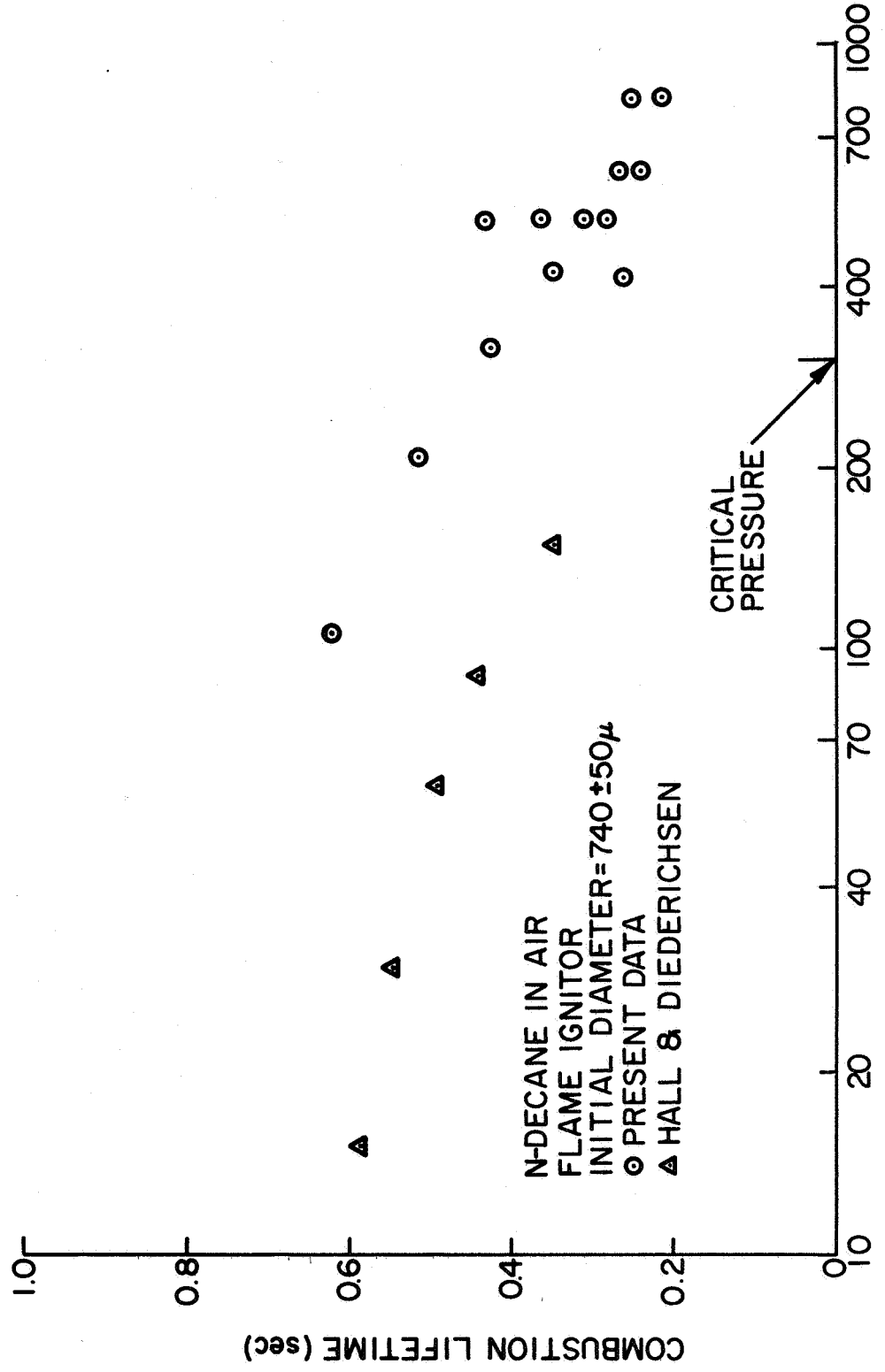

FIG. 7 COMBUSTION LIFETIME OF N-DECANE IN AIR-FLAME IGNITOR

Figure 8 shows combustion lifetimes for n-hexadecane (cetane). As before, the critical pressure was obtained from Reference 19. The trend of the lifetimes with pressure and the magnitude of the lifetimes are similar to the n-decane results.

Although these tests did allow observation of droplet combustion at pressures substantially above the critical pressure of the fuel, the results were not satisfactory. First, the high pressure combustion theories (14, 15) predict an increase in the burning lifetimes at pressures somewhat above the critical pressure of the fuel. The present data continues to exhibit a downward trend even at four times the critical pressure for cetane. Secondly, the films taken at high pressure, Figure 6, indicated that the fuel sample was being greatly distorted and possibly broken up by the ignitor flow. While this phenomenon is undoubtedly present in a combustion chamber, it presents a great problem in the analysis of this data. These factors prompted the use of the hot wire ignitor as a means of reducing the disturbance at ignition. The results of the hot wire ignitor tests are discussed in the next chapter.

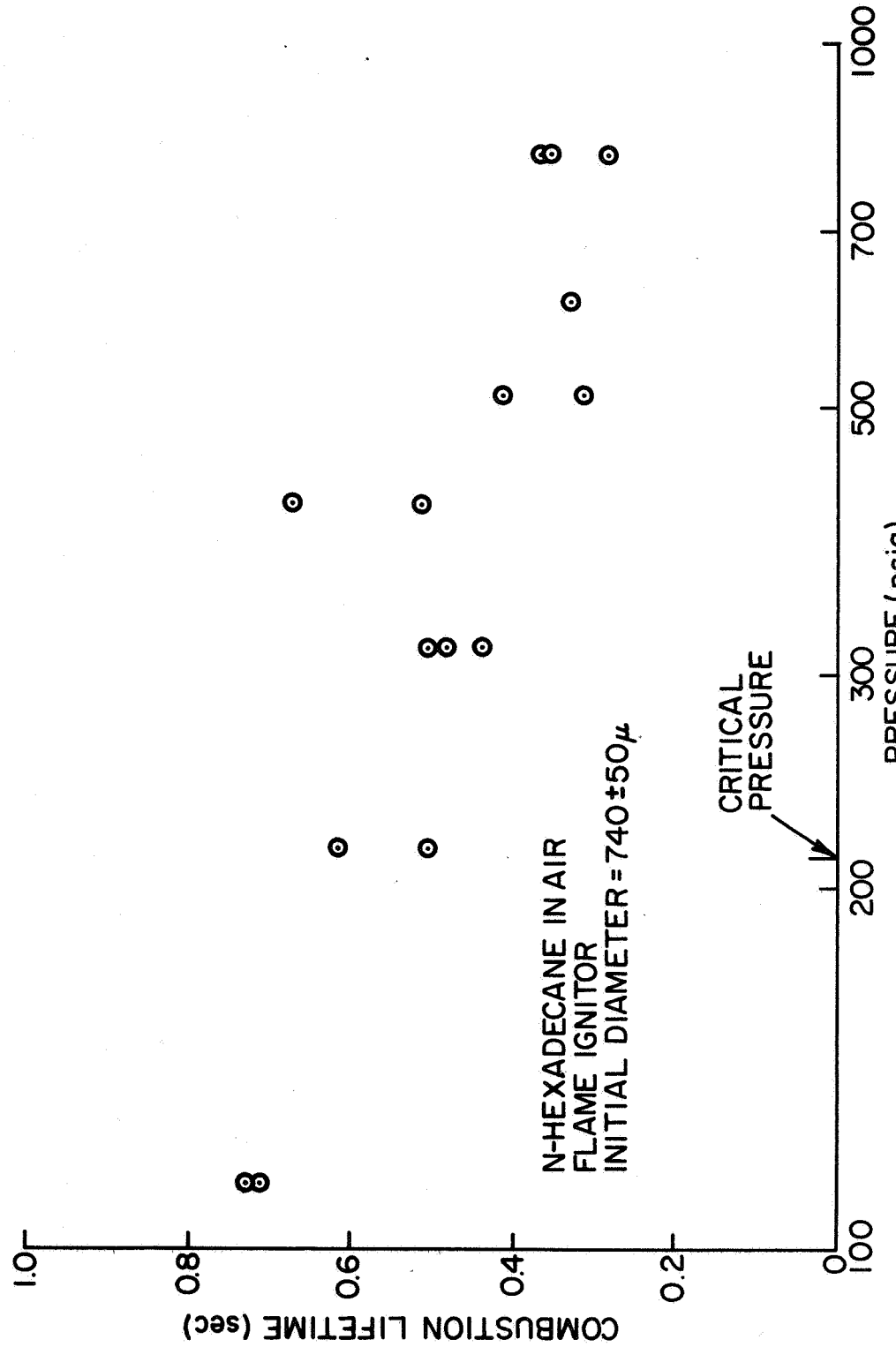

FIG. 8 COMBUSTION LIFETIME OF N-HEXADECANE IN AIR-FLAME IGNITOR

CHAPTER 4

RESULTS OF THE HOT WIRE IGNITOR TESTS

4.1 Combustion Lifetimes

For the tests with the hot wire ignitor, the droplet was mounted on the junction of a chromel alumel thermocouple and measurements of the droplet temperature were made. Figure 9 is a typical test at low pressures using the hot wire ignitor. The droplet fuel was n-decane which was burned in air at a pressure of 64 psia.

The first strip of film is the silhouette photograph of the droplet. The background light was a neon bulb which also permitted time correlation of the temperature trace and the films. After the background light goes off the hot wire ignitor begins to heat up and glow. It should be noted that the droplet does not ignite immediately after the wire begins glowing. When the droplet ignites, the disturbance is considerably less than what was observed during the flame ignitor tests. During combustion, the flame is almost spherical, not teardrop in shape as was seen in the flame ignitor photographs. This is due to the elimination of all convective effects including induced flows in the reaction chamber.

Figure 10 is an example of a test at high pressure using the hot wire ignitor. The test conditions consisted of an n-decane

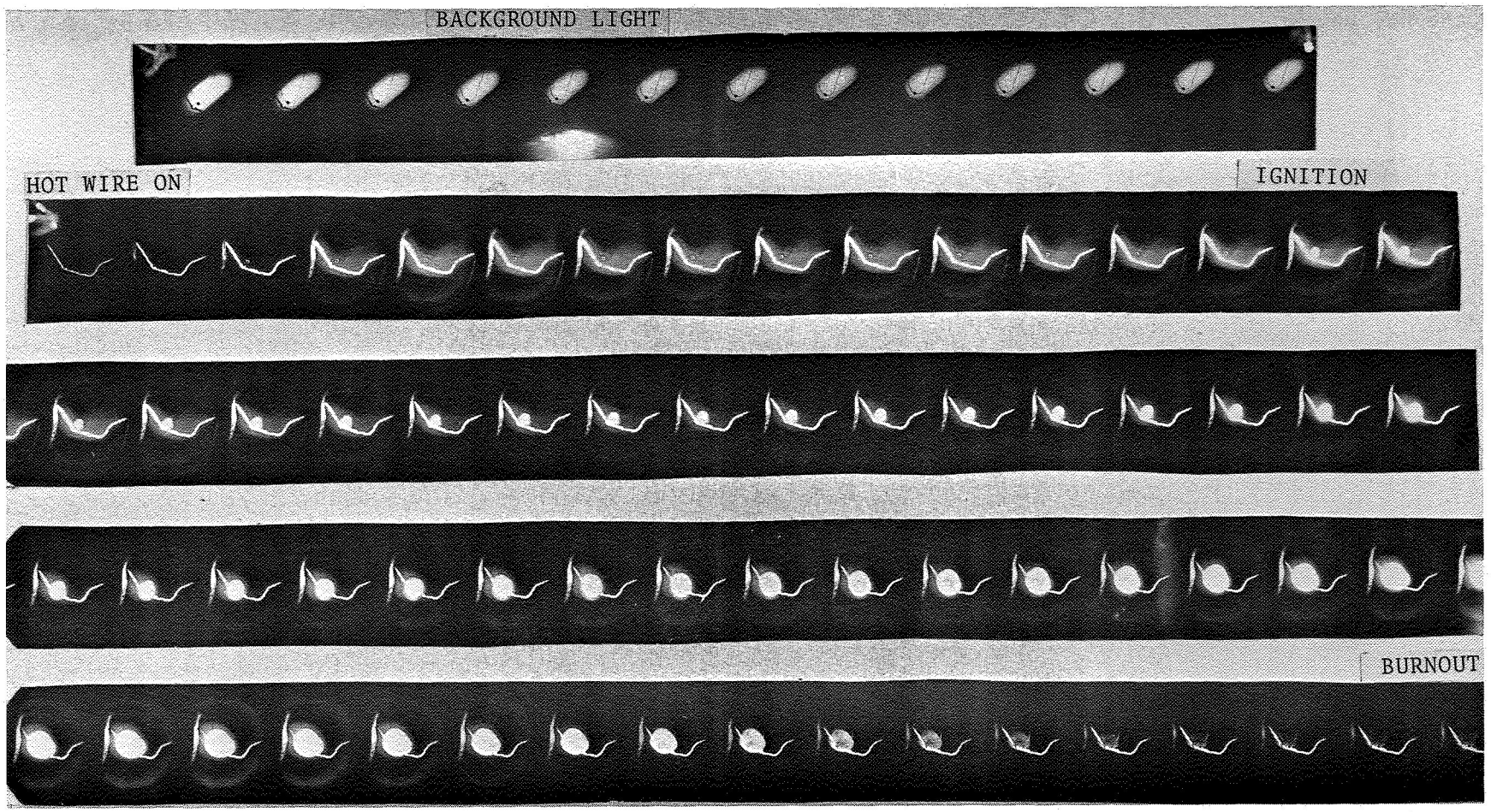

FIG. 9 COMBUSTION AT LOW PRESSURE (64 PSIA) WITH THE HOT WIRE IGNITOR

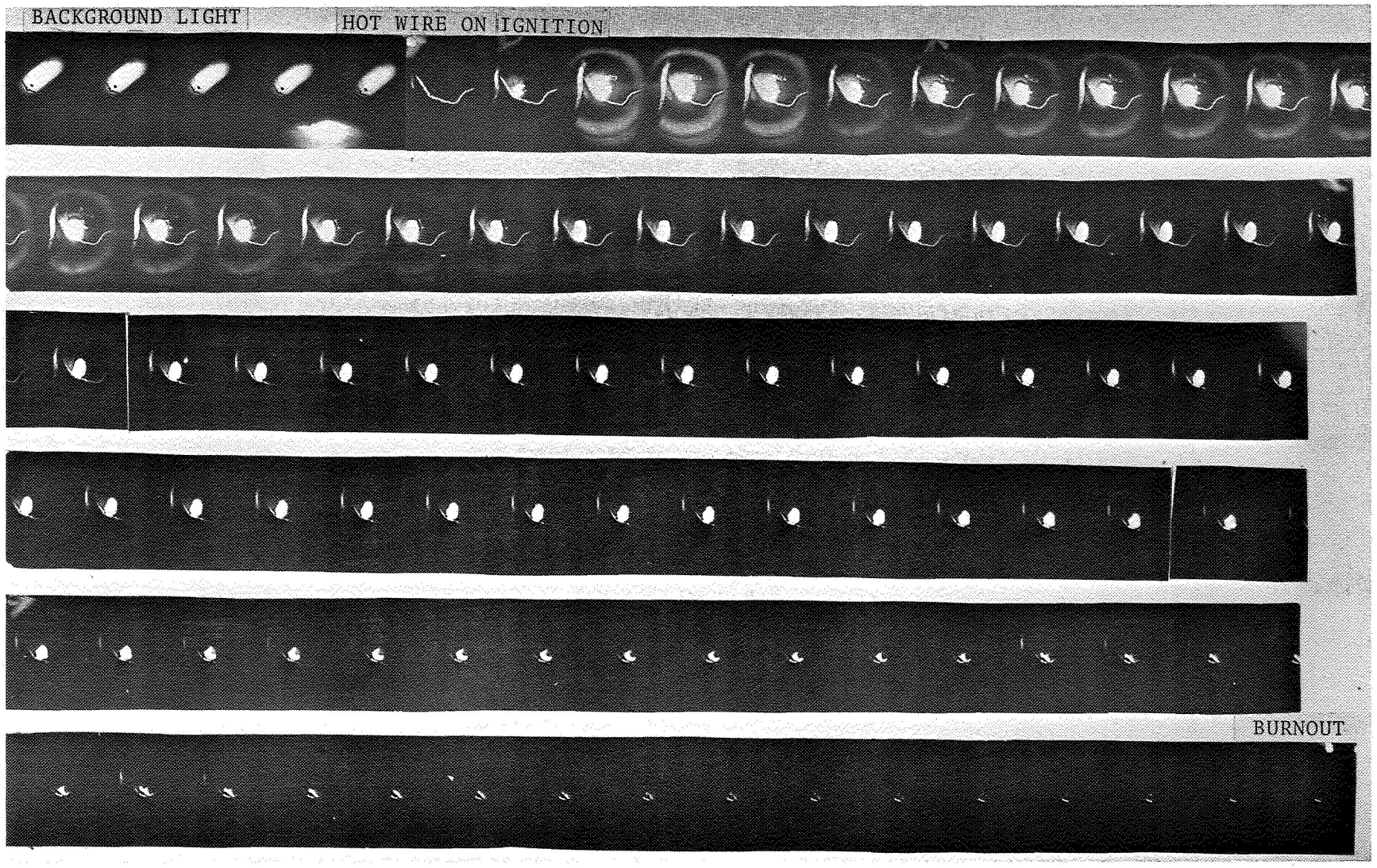

FIG. 10 COMBUSTION AT HIGH PRESSURE (814 PSIA) WITH THE HOT WIRE IGNITOR

droplet burning in air at 814 psia. At ignition, there is some disturbance but this quickly settles down to a steady flame zone. The disturbance is less severe than that observed in Figure 6, and shearing and distortion of the combustion zone is reduced. The droplet does not appear to leave the thermocouple location during the test. It is notable that the flame is much smaller than the flame observed in Figure 9, the low pressure test.

A plot of total combustion lifetime versus pressure for n-decane droplets using the hot wire ignitor is shown in Figure 11. The lifetimes were corrected to represent a fixed initial diameter droplet of 875 μ, since the range of actual diameters (533-899 μ) was broader than the range used in Figures 7 and 8. The correction assumed a squared relationship between the drop diameter and the combustion lifetime as follows:

$$t_c = (875/d)^2 \, t_m \qquad (3.1)$$

where d is the drop diameter in microns. The diameter squared correction was used since most of the separate processes undergone by the droplet, heat-up, steady burning, and supercritical burning are proportional to diameter squared (References 3-5, 14-16). The measured lifetime is the time between ignition and the end of luminosity of the droplet flame.

Comparing Figure 11 with Figure 7, it is seen that the trends are quite different for this set of data. Instead of monotonically decreasing lifetimes with increasing pressure, the lifetimes begin increasing somewhat above the critical pressure. This provides

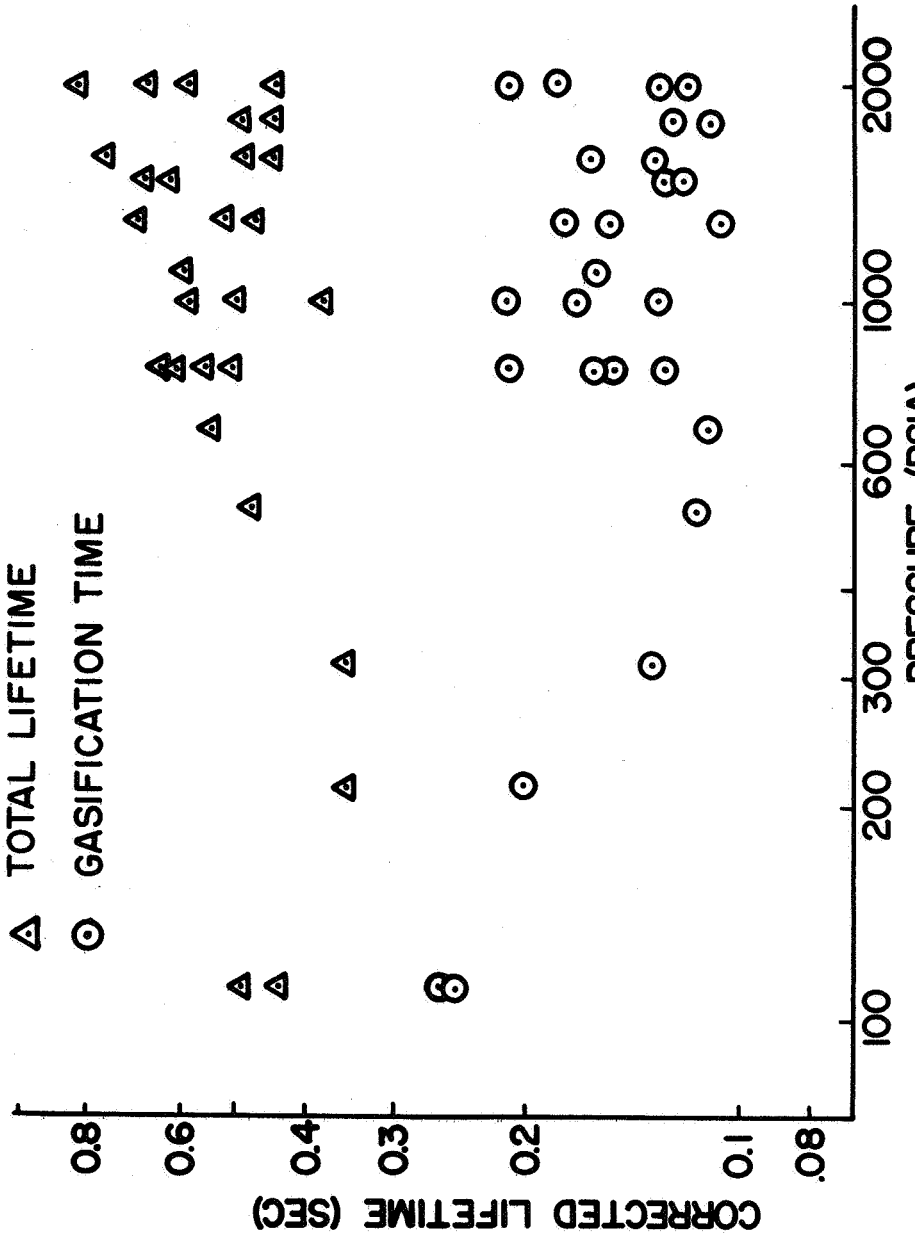

FIG. 11 COMBUSTION LIFETIME OF N-DECANE IN AIR-HOT WIRE IGNITOR (CORRECTED TO AN INITIAL DIAMETER OF 875 μ)

further evidence of the possibility that shearing and breakup of the droplet at ignition caused shortened lifetimes at high pressures when the flame ignitor was used.

Rosner (15) presents a qualitative picture of the pressure dependence of the droplet lifetimes for the various droplet combustion theories. In his discussion, the initial temperature of the droplet is taken to be the wet bulb temperature so that heat up is neglected. In the pressure region somewhat below the critical pressure, Rosner's quasi-steady prediction shows an almost constant burning lifetime with pressure. As the critical pressure is approached, the burning lifetime decreases, ultimately going to zero at the critical pressure for the simplest quasi-steady model (where the wet bulb temperature is taken to be the boiling temperature). For a model where evaporative sub-cooling of the droplet surface is included, the lifetime decreases as the critical pressure is approached, but remains finite at the critical pressure. From Figure 11 it is seen that the lifetimes do decrease as the critical pressure is approached and reach a minimum slightly above the critical pressure.

Considerably above the critical pressure of the fuel the supercritical burning theories (14, 15) predict the lifetimes to increase as the cube root of pressure. The data in Figure 11 shows lifetimes increasing, but there is a considerable amount of scatter in the data making it impossible to give more than a qualitative assessment of the pressure dependence of the burning lifetimes. Furthermore, total lifetimes include the time required for the

droplet to heat up from its temperature at ignition to either the wet bulb temperature for low pressure runs, or to the critical temperature at high pressures. Rosner's discussion concerns a droplet at its wet bulb temperature or a fuel sample at its critical temperature, and thus does not include the heat up period. It is, therefore, not physically correct to compare these results with theory at this point. This matter is discussed again in Section 4.3.

For pressures below 100 psia, the lifetimes were lower than Hall and Diederichsen's (16) data. At 114 psia Hall and Diederichsen's data overlaps the present data. It was felt that the data below 114 psia was overly influenced by excessive radiation from the hot wire and was, therefore, not included in the figure.

At low pressures, the hot wire glowed very brightly due to the low heat capacity of the surrounding air. The increased radiation caused higher heat transfer rates to the droplet. This would result in higher evaporation rates and, therefore, shorter lifetimes at low pressures. The effect of hot wire radiation will be further discussed in the next section.

4.2 Temperature Measurements

Temperature measurements of the liquid phase are subject to error due to temperature gradients in the droplet during heat up. However, the thermocouple gives a suitable representation of the droplet temperature (at least to a first approximation) and is, therefore, useful in rounding out the picture of droplet combustion.

A typical temperature trace is shown in Figure 12, for an n-decane droplet burning in air at 64 psia. The origin of the time axis is arbitrary. Marked on the time scale is the time when the hot wire begins glowing, the time when the droplet ignites and the time at the end of burning as obtained from the films. The series of peaks at the beginning of the trace is due to the noise signal sent to the thermocouple when power was first supplied to the hot wire.

The slope of the temperature trace increases shortly after ignition, which is characteristic of most of the tests. At the point of inflection the flame has apparently propagated its heating effect to the thermocouple location. The droplet temperature increases until the steady burning period is reached, whereupon the temperature remains constant. The trace remains at the wet bulb temperature until the droplet has completely gasified, then the temperature begins rising again until combustion is completed. Spalding (14) predicted that the end of burning occurs sometime after gasification of the droplet. The length of time from the end of gasification to the end of burning is surprisingly long even at low pressures. In Figure 12, it is roughly 40 percent of the total lifetime.

Figure 13 shows total lifetimes and times from ignition to the end of gasification (gasification times) plotted against pressure for droplets of n-decane. The triangles represent the total lifetimes and the circles are gasification times. The two sets of points diverge from each other with increasing pressure indicating that

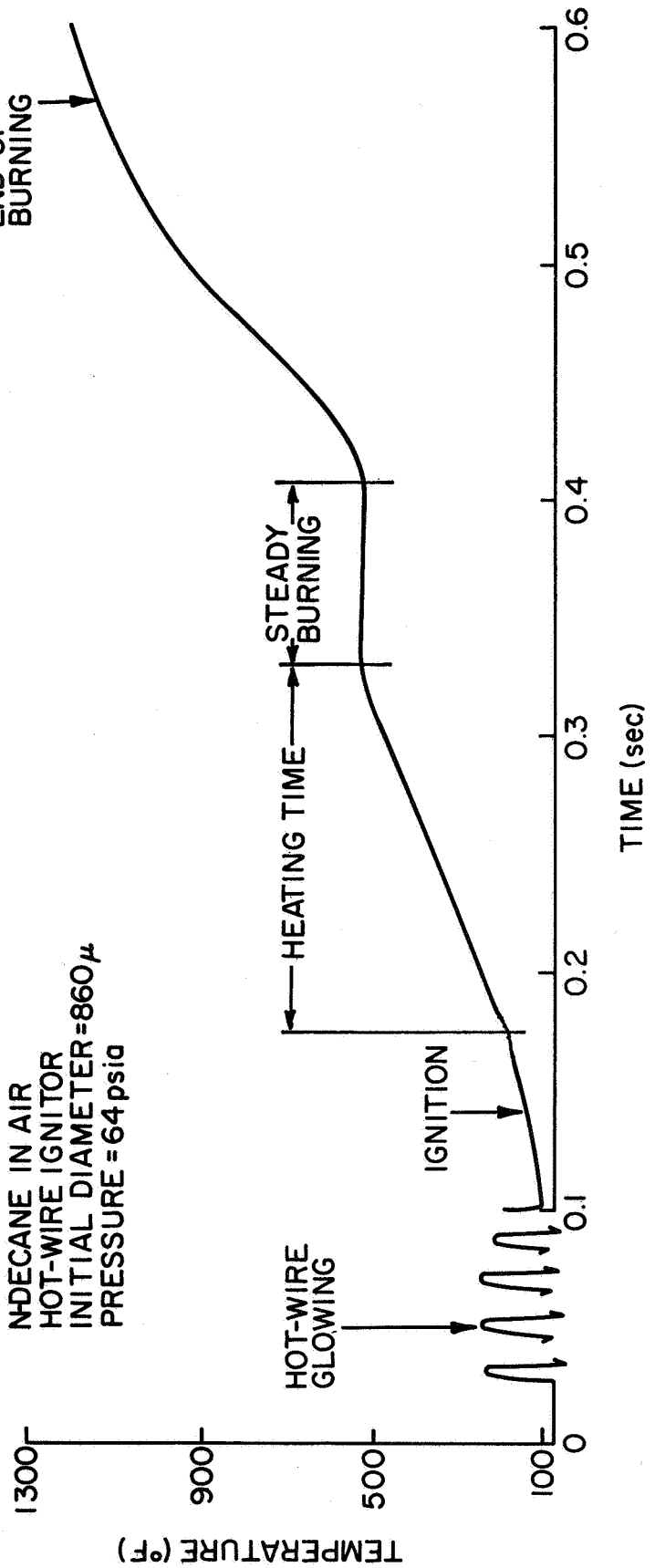

FIG. 12 TYPICAL TEMPERATURE RECORD

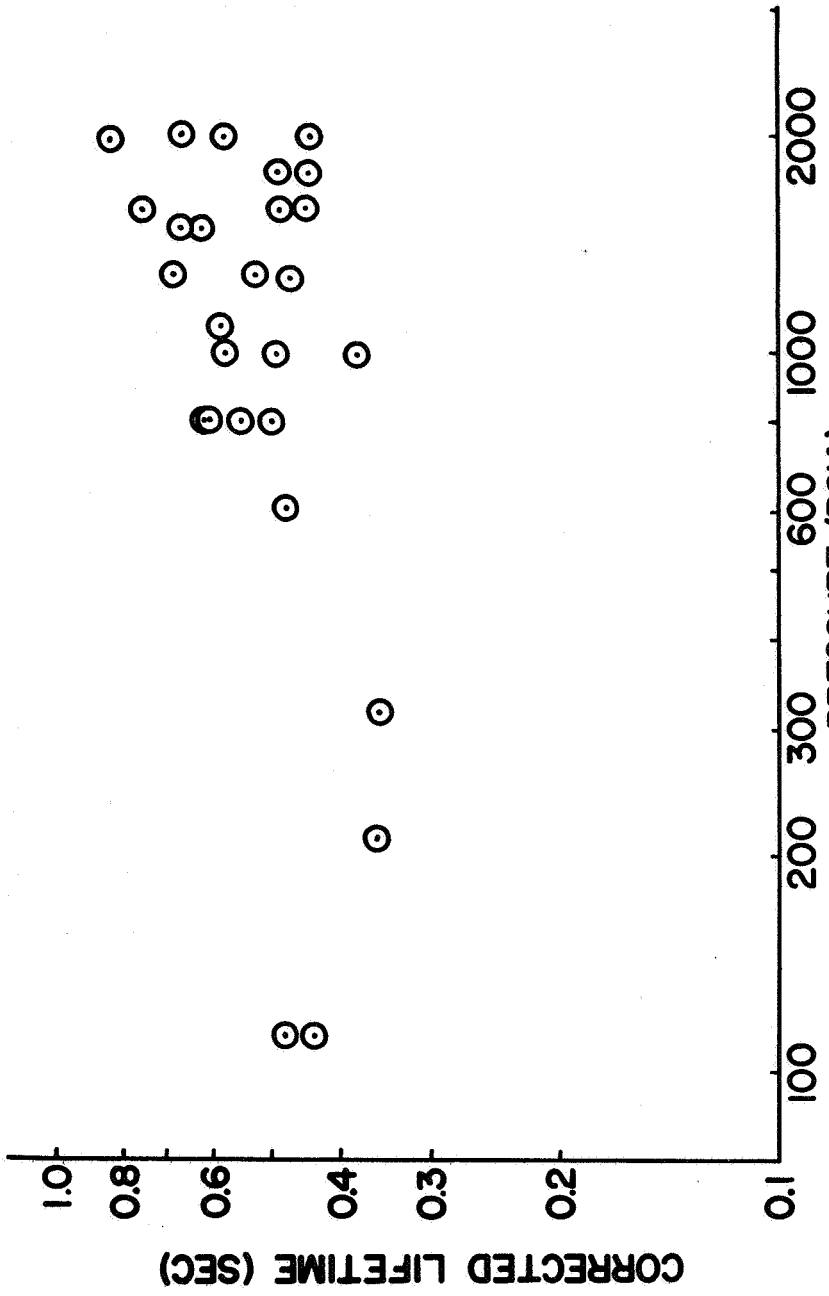

FIG. 13 GASIFICATION TIMES AND TOTAL LIFETIMES OF N-DECANE IN AIR-HOT WIRE IGNITOR (CORRECTED TO AN INITIAL DIAMETER OF 875 μ)

gasification of the droplet takes a smaller percentage of the total lifetime at higher pressures.

At 814 psia and above, the gasification time was taken to be the time between ignition and the instant the droplet reaches its critical temperature, which is obtained from the temperature trace. There is considerable scatter in this region (in part due to the fact that the droplet did not always ignite at the same liquid temperature) but there is a continued downward trend for the gasification times.

An important conclusion to be drawn from Figures 12 and 13 is that for the conditions of this experiment it is incorrect to interpret combustion lifetimes as gasification times for any pressure. It must be emphasized that convection plays a large part in the combustion of the gasified fuel, and may greatly decrease the time between the end of gasification and the end of burning. In a combustor with convection present, the increased rate of gas phase mixing may make this time extremely small. The results presented here should be taken as a worst case, where no convection is present due to the absence of gravity forces.

Figure 14 shows temperature traces at different pressures for droplets of n-decane. The critical temperature indicated on the trace was obtained from Reference 19. The times on the figure are plotted from the time of ignition.

The traces marked A, B, and C are traces for tests run at 114, 514, and 1100 psia, respectively. The droplet diameters for curves A, B, and C are 945, 990, and 947 microns, respectively.

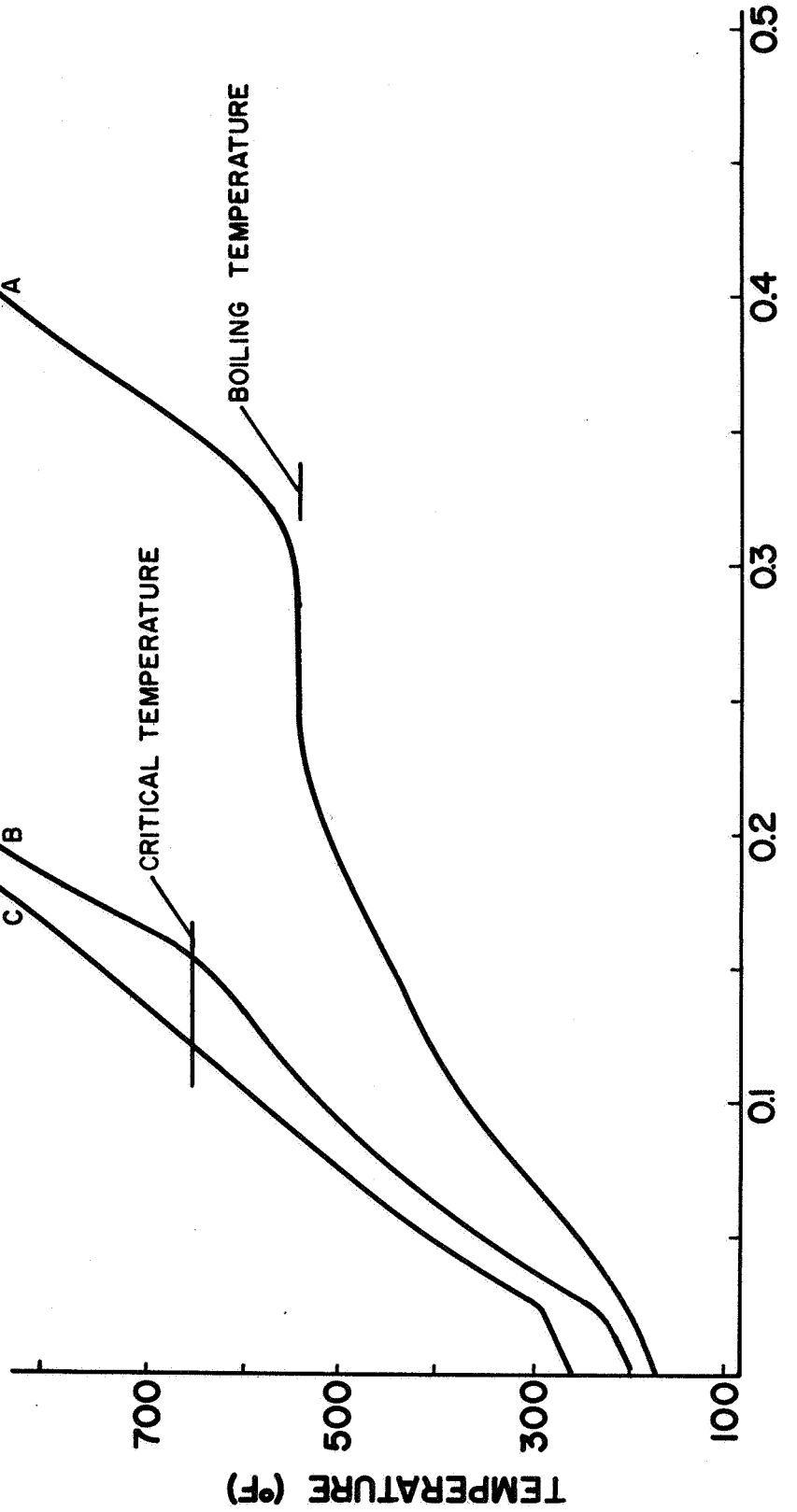

FIG. 14 DROPLET TEMPERATURE MEASUREMENTS AT VARIOUS PRESSURES

It was observed that with increasing pressure an n-decane droplet spends a smaller percentage of its burning lifetime in the steady burning period, characterized by the droplet's temperature remaining constant at the wet bulb temperature. Curve B, run at 514 psia shows an approach to the wet bulb state indicated by the inflection of the temperature trace. This type of behavior persisted to a pressure of 664 psia, even though this pressure is over twice the critical pressure. At 814 psia no inflection of the trace was observed, and the temperature record was similar to curve C in Figure 14 for tests at 814 psia and above. Apparently no approach to the wet bulb state was made by the droplet at these pressures.

It should also be noted from Figure 14, that the rate of temperature rise increases as pressure increases. This would agree with Wieber's (13) analysis which indicated that at high pressures a lower percentage of the total heat into the droplet from the flame is utilized for vaporization of the fuel and more of the heat is used for sensible heating of the droplet. Another characteristic of the results in Figure 14 is that the liquid temperature at ignition is higher as the ambient pressure is increased.

Also marked on Figure 14 is the boiling temperature (20) of n-decane for 114 psia. It should be noted that the wet bulb temperature is below the boiling temperature at this pressure. At pressures below 114 psia, however, liquid temperatures considerably above the boiling temperature were observed. Two possible causes of this are excessive radiation from the hot wire and conduction along the thermocouple wires. Either of these effects could

preferentially heat the thermocouple junction and cause high temperature readings.

A series of tests was run to determine the effect of hot wire radiation on the liquid temperature. The results are presented in Table 1. All tests were run at atmospheric pressure and the electrical power to the hot wire was varied. It is seen in Table 1 that for power levels below 1200 watts, the wet bulb temperatures remain fairly constant and are near the boiling temperature which is 344°F (19). However, at 1200 watts there is a jump in the maximum liquid temperature of about 50°F, indicating that the heater power does have an effect on temperature reading. The table also lends support to the possibility that excessive heater power was responsible for the short lifetimes at low pressures discussed in Section 4.1.

TABLE 1

HEATER POWER VERSUS MAXIMUM LIQUID TEMPERATURE

POWER (watts)	TEST NUMBER	MAXIMUM LIQUID TEMPERATURE (°F)
800	T-44	360
900	T-42	351
1000	T-40	344
1200	T-33, T-43	395, 437
1400	T-35	410

At higher pressures the heater power level was no longer a problem, due to the higher heat capacity of the air in the reaction chamber, which lowered the wire temperature. At high pressures, the power level was kept at 1600 watts, the minimum for consistent ignition.

The problem of conduction of heat along the thermocouple wires from the flame zone to the droplet is analyzed in Appendix C. A simplified model was used in the analysis and it was found that conduction along the thermocouple wires was responsible for about 15 percent of the heat transferred from the flame zone. The result points out the possibility that this effect could also be a factor causing the high liquid temperatures at very low pressures.

4.3 Supercritical Burning Lifetimes

The existing theories of supercritical burning (14, 15) model the fuel sample as a pocket of fuel vapor which is already above its critical point. Thus, the model does not account for heating the droplet from the ambient to the critical temperature. In view of this, there is no physical basis for comparing the results obtained in Figure 11 with the predictions of the supercritical burning theories.

Since droplet temperature measurements are available, it is possible to obtain the droplet's "supercritical burning lifetime" which is defined in this paper as the time between the instant the droplet reaches its critical temperature and the end of luminosity of the droplet's flame. The effect of using supercritical lifetimes

is to eliminate the heat up to the critical temperature and thus more closely represent Spalding's and Rosner's models.

When comparing the experimental results with the theory, it must be assumed that very little of the mass of the droplet is burned during heating to the critical temperature and thus the fuel mass present at the critical temperature is equal to the initial mass of the droplet. Wieber's (3) results indicate that at sufficiently high ambient pressures this is approximately the case. For example, for the combustion of an n-heptane droplet with an ambient pressure of four times the critical pressure, Wieber calculated that only eight percent of the initial mass of the droplet had vaporized by the time the droplet reached its critical temperature.

Figure 15 is a plot of supercritical lifetimes versus pressure for n-decane droplets. Again the lifetimes are corrected to equivalent lifetimes for an 875 micron droplet using the diameter squared correction discussed in Section 4.1. It should be noted that the lowest pressure represented on this plot is 814 psia, since at this pressure no inflection of the temperature trace was observed and thus apparently no approach to the wet bulb state was made by the burning droplet. An approach to the wet bulb state would indicate a significant amount of vaporization during heating.

To obtain agreement between the data and the theories (14, 15) the observed supercritical lifetimes should increase as the cube root of pressure. On the log-log plot of Figure 15, the data should follow a line with a 1/3 slope.

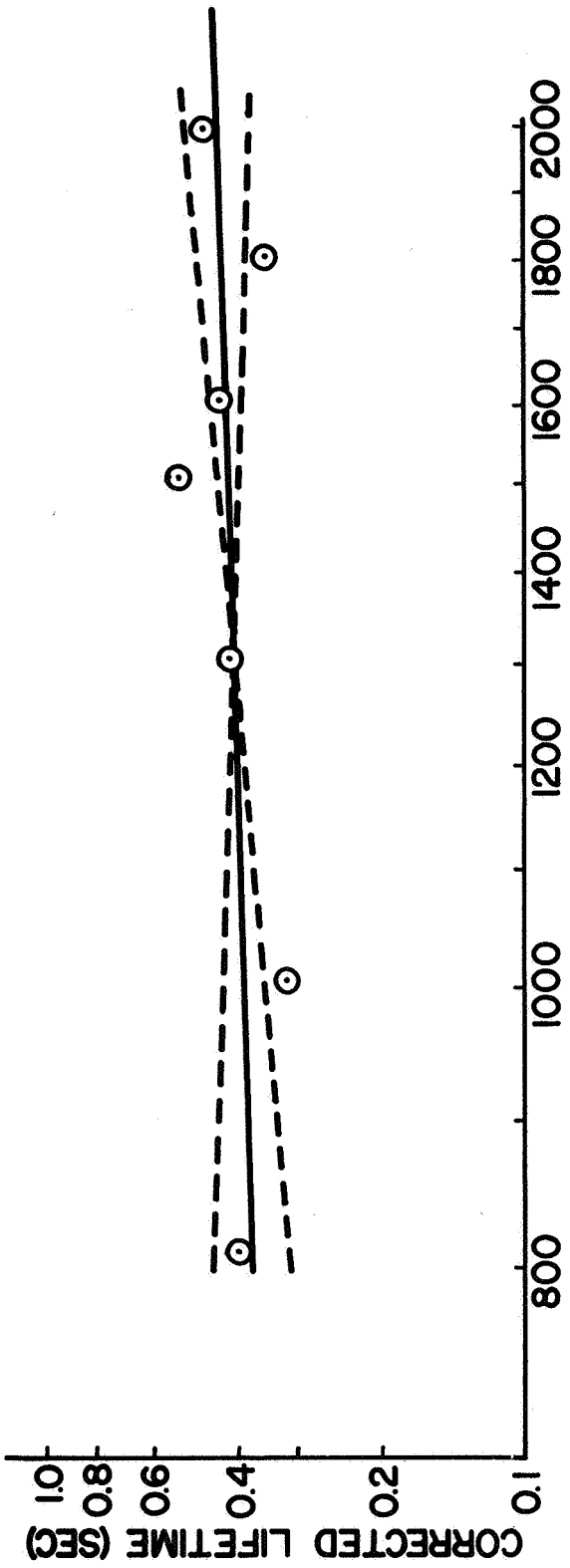

FIG. 15 SUPERCRITICAL BURNING LIFETIMES OF N-DECANE IN AIR (CORRECTED TO AN INITIAL DIAMETER OF 875 μ)

The original data were highly scattered, and in order to make a comparison, only the average at each pressure is shown in Figure 15. At all pressures except 1814 psia, the averages were of two or more tests. In addition, a least squares regression line was fitted to all the original data. The slope of the regression line was 0.18 which is lower than the theories (14, 15) predict.

A statistical analysis was done on this data sample in order to obtain confidence limits on the slope of the regression line. At a 95 percent confidence level the slope of the line falls between -0.19 and 0.55, which is indicated on the figure by the dotted lines. It would be expected to a 95 percent level of confidence that if a larger series of tests were run on this apparatus the slope of the regression line fitted to this large sample would fall within these limits. The slope 1/3 falls in this confidence interval indicating that at the 95 percent confidence level there is no statistically significant difference between the slope 1/3 and the slope of the regression line, 0.18.

It was apparent on examination of the original data that the lifetimes at 814 psia were rather high in comparison to the lifetimes at 1014 and 1114 psia. This was possibly due to a reduced level of ignition disturbance at 814 psia compared to the higher pressure data. This could be a factor contributing to the flatness of the least squares line shown in Figure 15. It is interesting to note that if the 814 psia data is removed and a regression line is fitted to the remaining data, the resulting slope is 0.372. However, the confidence limits for this data are much wider than those

in Figure 15, and since no basis could be found for eliminating the 814 psia data, the flatter least squares line was kept as representative of the present experiment.

4.4 Comparison of Theory with Experimental Results

The final step in evaluating the data consisted of a comparison between the supercritical combustion theories (14, 15) and the experimental data. Rosner (15) presents a graph showing the non-dimensionalized burning time as a function of ν, the stoichiometry parameter, for his theory and for Spalding's (14) theory. The graph is shown in Figure 16. Spalding's result is represented by the straight line, Rosner's by the curve. For very small values of the stoichiometry parameter the models tend to converge, however, at larger values of ν, Spalding's model always predicts a considerably larger non-dimensional burning time. The stoichiometry parameter depends primarily on the reaction, and for n-decane burning in air $\nu = 0.0665$. The resultant dimensionless burning times are 1.21 for Rosner's theory and 1.30 for Spalding's.

The dimensionless burning time plotted in Figure 16 is defined in Reference 15 as

$$\tau_b = t_b \frac{D_{12}}{a^2} \quad . \tag{4.1}$$

Thus, to dimensionalize these numbers, the equivalent fuel radius, a, and the binary diffusion coefficient, D_{12}, must be found. The definition of the equivalent radius, a, comes from the equation

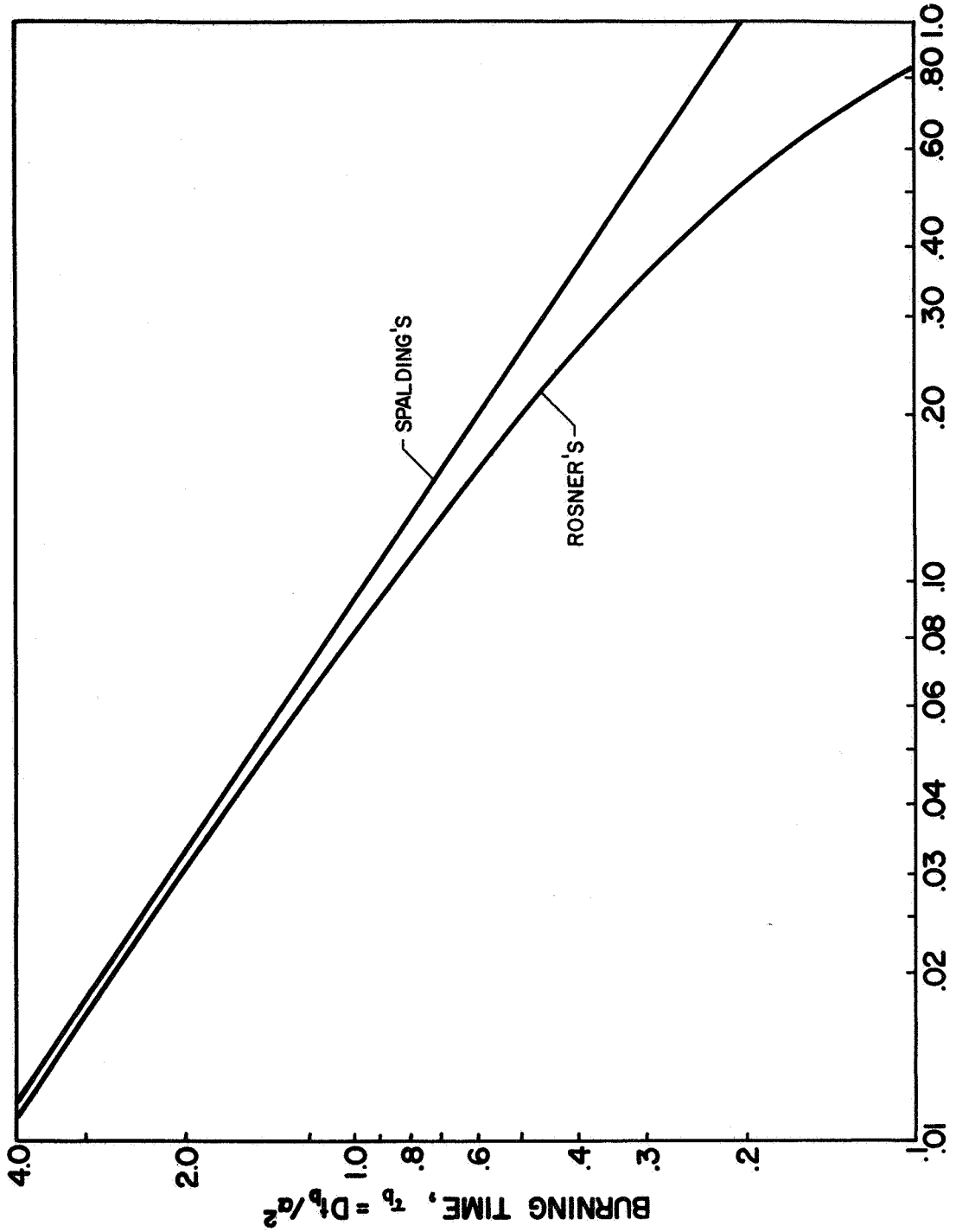

FIG. 16 DIMENSIONLESS THEORETICAL BURNING LIFETIME

$$W_f = \frac{4}{3} \pi \rho a^3 \tag{4.2}$$

since

$$W_f = \frac{4}{3} \pi \rho_\ell r_\ell^3 \tag{4.3}$$

then

$$a^3 = \frac{\rho_\ell}{\rho} r_\ell^3 \quad . \tag{4.4}$$

The surrounding gas density, ρ, was evaluated using the ideal gas law at T = 4000°R, the approximate flame temperature (21) and the ambient chamber pressure. The average of the molecular weights of n-decane and air was used in the evaluation of the gas constant used in the ideal gas equation. The value of ρ_ℓ was taken to be 45.5 lb_m/ft^3 (19) and the average droplet radius r_ℓ was 438 microns from the initial diameter used to normalize the measured lifetimes. Table 2 shows values of ρ, a, and D_{12} for each pressure at which the calculations were made.

The diffusion coefficient was calculated using two methods described in Reference 22. The first, recommended by Hirschfelder, Curtiss and Bird (23), is given by the following equation:

$$D_{12} = \frac{0.001858\ T^{3/2}\ [(M_1 + M_2)/M_1M_2]^{1/2}}{P\rho_{12}^2\ \Omega_d} \quad . \tag{4.5}$$

The second method was due to Slattery (24) and is given by

$$D_{12} = \frac{2.74 \times 10^{-4}}{P} \frac{T^{1.823}}{(T_{cr_1}T_{cr_2})^{1/2}} (P_{cr_1}P_{cr_2})^{1/3}$$

$$(T_{cr_1}T_{cr_2})^{5/12}\ [(M_1 + M_2)/M_1M_2]^{1/2} \quad . \tag{4.6}$$

TABLE 2

VALUES USED IN THE THEORETICAL FIT

p (psia)	ρ lb_m/ft^3	a (microns)	D_{12} (Ref. 23) (cm^2/sec)	D_{12} (Ref. 24) (cm^2/sec)
814	3.243	1057	0.0342	0.0417
1014	4.040	983	0.0275	0.0334
1114	4.439	952	0.0250	0.0304
1314	5.236	902	0.0212	0.0258
1514	6.032	860	0.0184	0.0224
1614	6.431	843	0.0172	0.0210
1814	7.228	808	0.0154	0.0187
2014	8.025	781	0.0138	0.0168

Equations (4.5) and (4.6) were used to calculate the diffusion coefficients at 4000°R and one atmosphere pressure. A high pressure correction by Slattery (24) was used which was based on reduced properties. However, at high reduced temperatures the correction reduces to

$$\frac{(D_{12}\ P)}{(D_{12}\ P)_{1\ atm}} \simeq 1.0 \quad . \tag{4.7}$$

Thus, the high pressure diffusion coefficient is inversely proportional to pressure. It must be emphasized here that Equation (4.7) gives a rough estimate for the high pressure diffusion coefficient since no reliable calculation method exists at the present time.

A plot of theoretical burning times is shown in Figure 17, which also shows the experimental data and the least squares line for the data. The least squares line is indicated by the solid line. The best agreement for the theoretical lines is obtained using Slattery's (24) method for calculating the low pressure diffusion coefficient. The lines marked PS and DS indicate Spalding's point source and Rosner's distributed source models. The slope of the theoretical line is always one-third, which is higher than the slope of the least squares line, but is within the 95 percent confidence limits of the data as discussed previously.

Differences between Spalding (14) and Rosner's (15) theories are very small for these conditions with Spalding's theory predicting a somewhat longer burning time. The difference between the two theories is greater as ν gets larger, which corresponds to an oxidant rich environment for the droplet.

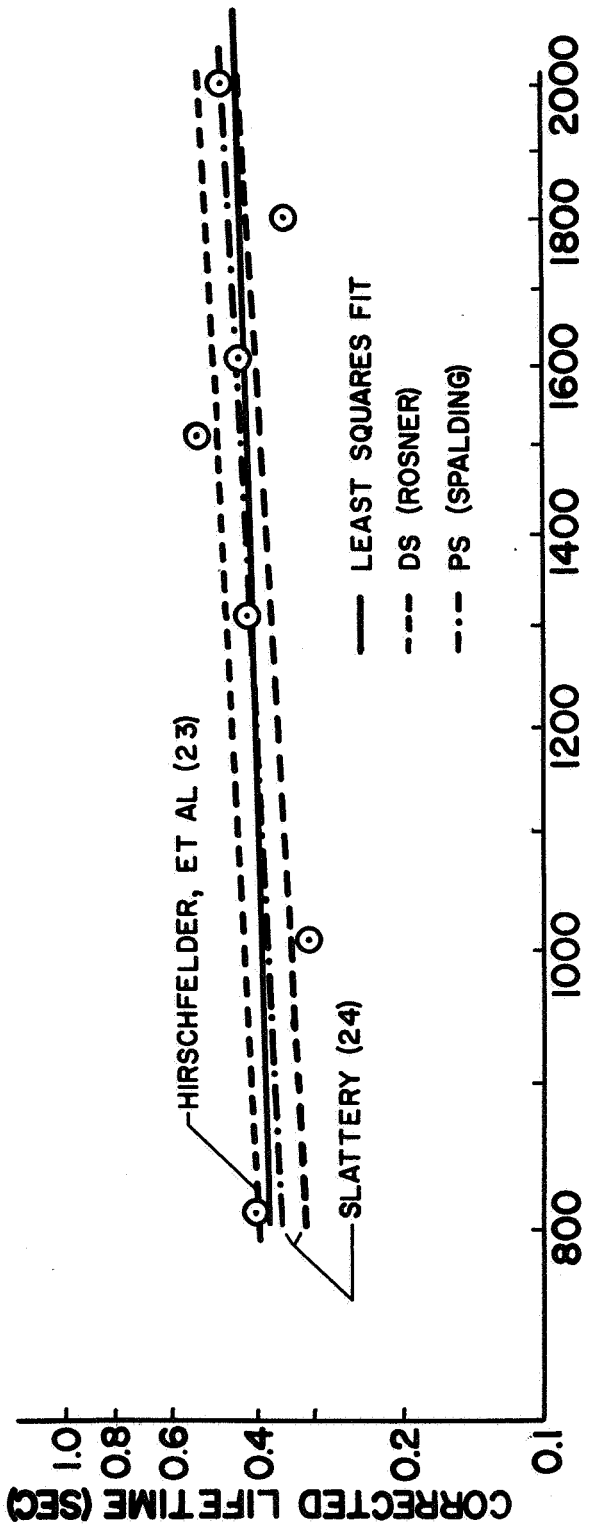

FIG. 17 THEORETICAL AND EXPERIMENTAL SUPERCRITICAL BURNING TIMES

CHAPTER 5

SUMMARY

An experimental study of the combustion of bipropellant droplets in air was undertaken. The primary objectives of the experiment were to study the combustion of single supported droplets under pressures which would produce near critical and supercritical burning and to compare the quasi-steady and supercritical combustion theories with the experimental results. Necessary modifications were to be made on the theories in order to obtain reliable predictions for droplet life histories.

The experimental apparatus permitted measurement of burning lifetimes and droplet temperatures under zero gravity conditions by means of a free fall apparatus. The presence of zero gravity conditions eliminated the problem of the droplet falling from its support near the critical point due to reduced surface tension and also eliminated the effects of natural convection in the system. The fuels used were n-decane and n-hexadecane. Two methods were used to ignite the droplets; the first consisted of directing a small hydrogen diffusion flame toward the droplet, the second method employed an electrically heated wire to directly ignite the droplet.

The conclusions of the study were as follows:

1. Supercritical burning was observed using the methods of the experiment.

2. The analyses of Spalding (14) and Rosner (15) agree adequately with the experimental data. A method of determining the average properties employed in the theories was found which matched the theory to the experimental burning times.
3. Conditions where droplet gasification occurs almost entirely in the supercritical mode were found, which qualitatively substantiated the predictions of Wieber (13).
4. It was found that for the conditions of this experiment, it is incorrect to interpret gasification lifetimes as combustion lifetimes for all pressures tested. Also it was found that the time from droplet ignition to total gasification decreased as pressure was increased.
5. It was found that at high pressures a decane droplet spends a smaller fraction of its burning lifetime in the steady burning period, characterized by the droplet remaining at its "wet bulb" temperature. An approach to the wet bulb state was observed at pressures over twice as high as the critical pressure of n-decane.
6. At high pressures, the flame ignitor caused a great amount of disturbance at droplet ignition and throughout the combustion process. This resulted in questionable values for combustion lifetimes.

The hot wire ignitor greatly improved this situation and was judged the better of the two ignitor systems.

7. Comparison of the results with the flame ignitor and hot wire ignitor indicates that the presence of convection causes a substantial reduction of combustion time. The influence of convection is an aspect of supercritical combustion that deserves further study.

APPENDIX A

DERIVATION OF THE SUPERCRITICAL BURNING EQUATIONS

A.1 Introduction

The following appendix presents a detailed derivation of the theory of supercritical combustion due to Spalding (14) and the modification of the theory by Rosner (15). The analysis presented here differs from Spalding's somewhat because the basic equations used by Spalding are based on the conservation of an element. The equations used in this appendix are based on the conservation of a chemical compound.

The equations obtained in the following derivation differ from the equations used in the quasi-steady theory in that the radial convection term is eliminated but the transient term is retained in the equation of species conservation. The difference between the Spalding and Rosner models is due to the fact that Spalding assumes that the fuel vapor diffuses into the flame zone from a point source, while Rosner gives finite dimensions to the source.

The basic model consists of a pocket of fuel vapor surrounded by a spherical flame zone. Outside of the flame zone is an environment containing oxidant. Fuel diffuses outward to the flame zone and oxidant diffuses inward to the flame where they are instantly reacted to form products of combustion.

A.2 Spalding's Model (14)

The following assumptions are made in Spalding's analysis:

1. Fluid properties are constant.
2. Mass diffusivities of all species are identical and only concentration diffusion is present in the system.
3. Radial convection is negligible, i.e. the radial bulk velocity is zero.
4. Body forces are neglected.
5. The chemical reaction can be represented by a single, one step reaction

$$\nu_F W_F + \nu_O W_O \rightarrow \nu_P W_P \quad .$$

6. The reaction takes place in a thin flame zone.
7. Only three components comprise the system: fuel, oxidant, and combustion products.

The conservation equations are obtained from Williams (25). The conservation of species i is given by

$$\rho \frac{\partial Y_i}{\partial t} = w_i - [\nabla \cdot (\rho Y_i \vec{V}_i)] \quad . \tag{A.1}$$

The constitutive diffusion relation is

$$\nabla X_i = \sum_{j=1}^{N} \left(\frac{X_i X_j}{D_{ij}} \right) (\vec{V}_j - \vec{V}_i) \quad . \tag{A.2}$$

The phenomonological chemical kinetic expression is

$$w_i = W_i \sum_{k=1}^{M} (\nu''_{i,k} - \nu'_{i,k})\, B_k T^{\alpha_k} \exp\left(\frac{-E_k}{R^\circ T}\right) \prod_{j=1}^{N} \left(\frac{X_j P}{R^\circ T}\right)^{\nu'_{j,k}} \qquad (A.3)$$

$$i = 1, \ldots, N \quad .$$

Applying the assumption that the binary diffusivities are equal in (A.2) and rearranging according to Williams (25) yields

$$\vec{V}_i = -D \nabla \ell n Y_i \qquad (A.4)$$

or

$$\vec{V}_i = -D \frac{\nabla Y_i}{Y_i} \quad . \qquad (A.5)$$

Substituting (A.5) into (A.1) gives

$$\rho \frac{\partial Y_i}{\partial t} = w_i + \nabla \cdot (\rho D \nabla Y_i) \quad . \qquad (A.6)$$

For a single, one step reaction Equation (A.3) becomes

$$w_i = W_i (\nu''_i - \nu'_i)\, B T^{\alpha} \exp\left(\frac{-E}{R^\circ T}\right) \prod_{j=1}^{N} \left(\frac{X_j P}{R^\circ T}\right)^{\nu'_j} \quad . \qquad (A.7)$$

since

$$\omega = B T^{\alpha} \exp\left(\frac{-E}{R^\circ T}\right) \prod_{j=1}^{N} \left(\frac{X_j P}{R^\circ T}\right)^{\nu'_j} \qquad (A.8)$$

then

$$w_i = W_i (\nu''_i - \nu'_i)\, \omega \quad . \qquad (A.9)$$

Substituting this expression into (A.6) yields

$$\rho \frac{\partial Y_i}{\partial t} - \nabla \cdot (\rho D \nabla Y_i) = W_i (\nu''_i - \nu'_i)\, \omega \qquad (A.10)$$

Defining

$$\alpha_i \equiv \frac{Y_i}{W_i(\nu_i'' - \nu_i')} \tag{A.11}$$

and substituting this expression into (A.10) gives

$$\rho \frac{\partial \alpha_i}{\partial t} - \nabla\cdot(\rho D \nabla \alpha_i) = \omega \qquad i = 1, \ldots, N \ . \tag{A.12}$$

Now the subscripts F, O, and P will represent fuel, oxidant, and products respectively. Letting

$$\beta' \equiv \alpha_P - \alpha_F \tag{A.13}$$

gives

$$\beta' = \frac{Y_P}{\nu_P W_P} + \frac{Y_F}{\nu_F W_F} \ . \tag{A.14}$$

Substituting (A.13) for α_P in (A.12) and using (A.12) to eliminate the reaction term, ω, yields

$$\rho \frac{\partial \beta'}{\partial t} - \nabla\cdot(\rho D \nabla \beta') = 0 \ . \tag{A.15}$$

The following quantities may be defined

$$\beta_0' = \beta'(r \leq a, \ t = 0) \tag{A.16}$$

or

$$\beta_0' = \frac{1}{\nu_F W_F} \tag{A.17}$$

and

$$\beta_\infty' = \beta'(r \to \infty) \tag{A.18}$$

or

$$\beta'_\infty = \frac{Y_{P\infty}}{\nu_P W_P} \quad . \tag{A.19}$$

It is assumed that the gas far from the droplet has some constant concentration of products, $Y_{P\infty}$. Now letting

$$\Gamma \equiv \frac{\beta' - \beta'_\infty}{\beta'_0 - \beta'_\infty} \tag{A.20}$$

and substituting (A.20) into (A.15) yields

$$\rho \frac{\partial \Gamma}{\partial t} - \nabla\cdot(\rho D \nabla \Gamma) = 0 \quad . \tag{A.21}$$

In spherical coordinates (A.21) becomes

$$\rho \frac{\partial \Gamma}{\partial t} - \frac{D\rho}{r^2} \frac{\partial}{\partial r} \left(r^2 \frac{\partial \Gamma}{\partial r}\right) = 0 \quad . \tag{A.22}$$

The first boundary condition applies at very large radius.

At

$$r \to \infty \qquad \Gamma = 0 \tag{A.23}$$

since

$$\beta' = \beta'_\infty \qquad \text{at} \qquad r \to \infty \quad .$$

The second boundary condition arises from the fact that the total amount of fuel in the system is constant (either as fuel or reacted to form products). This can be written as

$$W_t = \int_0^\infty 4\pi r^2 \rho \left(Y_F + \frac{\nu_F W_F}{\nu_P W_P} Y_P\right) dr \quad . \tag{A.24}$$

The initial amount of fuel in the system is

$$W_{in} = \int_a^\infty 4\pi r^2 \rho \frac{\nu_F W_F}{\nu_P W_P} Y_{P\infty} \, dr + W_f \qquad (A.25)$$

where W_f is the mass of fuel injected in at t = 0. W_f is given by

$$W_f = \int_0^a 4\pi \rho r^2 \, dr \quad . \qquad (A.26)$$

However, when W_f is injected into the system, it displaces an amount of the ambient fuel (which exists as products) equal to

$$\int_0^a 4\pi r^2 \rho \frac{\nu_F W_F}{\nu_P W_P} Y_{P\infty} \, dr \quad . \qquad (A.27)$$

This amount must be subtracted out in Equation (A.25). Thus, substituting (A.26) into (A.25) and subtracting (A.27) yields

$$W_{in} = \int_0^\infty 4\pi r^2 \rho \frac{\nu_F W_F}{\nu_P W_P} Y_{P\infty} \, dr + \int_0^a 4\pi r^2 \rho \left(1 - \frac{\nu_F W_F}{\nu_P W_P} Y_{P\infty}\right) dr \quad . \qquad (A.28)$$

Since $W_{in} = W_t$, (A.24) may be combined with (A.28) also using (A.26) to yield

$$\int_0^\infty 4\pi r^2 \rho \left(Y_F + \frac{\nu_F W_F}{\nu_P W_P} Y_P\right) dr = \int_0^\infty 4\pi r^2 \rho \frac{\nu_F W_F}{\nu_P W_P} Y_{P\infty} \, dr + W_f \left(1 - \frac{\nu_F W_F}{\nu_P W_P} Y_{P\infty}\right) \quad . \qquad (A.29)$$

Solving (A.29) for W_f and noting that

$$\Gamma = \frac{Y_F + \frac{\nu_F W_F}{\nu_P W_P}(Y_P - Y_{P\infty})}{1 - \frac{\nu_F W_F}{\nu_P W_P} Y_{P\infty}} \tag{A.30}$$

gives

$$W_f = \int_0^\infty 4\pi r^2 \rho \Gamma \, dr \tag{A.31}$$

for the second boundary condition.

The initial condition is that at $t = 0$ and $r \leq a$ the fuel mass fraction is 1. For $r > a$, the concentration of products is simply the ambient concentration $Y_{P\infty}$. In terms of the variable, Γ, the initial condition becomes

$$t = 0 \quad , \quad r \leq a \quad , \quad \Gamma = 1 \tag{A.32}$$

$$t = 0 \quad , \quad r > a \quad , \quad \Gamma = 0 \quad . \tag{A.33}$$

At this point, Spalding produces a particular solution for (A.22) and the boundary conditions. The solution is the following:

$$\Gamma = \frac{W_f}{\rho(4\pi Dt)^{3/2}} \exp\left(\frac{-r^2}{4Dt}\right) \quad . \tag{A.34}$$

Spalding then notes, that for times of order greater than a^2/D the fuel distribution is independent of whether the initial mass is concentrated at a point or is finitely distributed. He therefore uses Equation (A.34) without the initial condition, and notes that (A.34) is unrealistic at very short times.

Examining conditions at the flame, where $Y_F = 0$, $Y_O = 0$ and $Y_P = 1$ and noting that

$$Y_{P\infty} + Y_{O\infty} = 1 \tag{A.35}$$

and

$$\nu_F W_F + \nu_O W_O \rightarrow \nu_P W_P \tag{A.36}$$

then

$$\Gamma_f = \frac{Y_{O\infty}}{\frac{\nu_O W_O}{\nu_P W_P} + Y_{O\infty}} \quad . \tag{A.37}$$

Solving (A.34) for r when $\Gamma = \Gamma_f$ yields the flame position as a function of time

$$\frac{r_f^2}{4Dt} = \ell n \left(\frac{W_f}{\rho \Gamma_f (4\pi Dt)^{3/2}} \right) \quad . \tag{A.38}$$

Defining the following dimensionless quantities

$$\phi \equiv \frac{r_f}{(W_f/\rho\Gamma)^{1/3}} \tag{A.39}$$

$$\theta \equiv \frac{4\pi Dt}{(W_f/\rho\Gamma)^{2/3}} \tag{A.40}$$

and substituting into (A.35) yields for the dimensionless flame radius

$$\phi = \left[- \left(\frac{3}{2\pi}\right) \theta \ \ell n \ \theta \right]^{1/2} \tag{A.41}$$

differentiating (A.41) and setting the derivative equal to zero gives the maximum value of ϕ.

$$\phi_{max} = 0.419 \tag{A.42}$$

where

$$\theta = 0.368 \tag{A.43}$$

thus the maximum flame radius is

$$r_{f\ max} = 0.419\ (W_f/\rho\Gamma)^{1/3} \quad . \tag{A.44}$$

At the end of burning $r_f = 0$, and therefore $\phi = 0$. When $\phi = 0$, $\theta = 1$. Substituting $\theta = 1$ into (A.40) yields

$$t_b = \frac{(W_f/\rho\Gamma)^{2/3}}{4\pi D} \quad . \tag{A.45}$$

To obtain the pressure dependence of the burning lifetime, the above equation can be multiplied by ρ/ρ. Noting that the product (ρD) remains constant with pressure (14) yields

$$t_b = \frac{\rho^{1/3}(W_f/\Gamma)^{2/3}}{4\pi(\rho D)} \quad . \tag{A.46}$$

Since ρ is proportional to pressure, the burning time is proportional to the cube root of pressure. It is also important to note from Equation (A.43) that the burning time is proportional to the two-thirds power of the initial droplet mass, and is therefore proportional to the square of the initial droplet radius.

A.3 Rosner's Solution (15)

Rosner's solution of the supercritical droplet combustion problem involves the same assumptions and the same differential equation, (A.22), developed in the preceding section. Rosner, however, does not neglect the initial condition as Spalding does. Because of this additional simplification Spalding indicates that his solution is not applicable for times of order less than a^2/D. Thus, for short burning times, which would occur in an oxidant rich environment, Spalding's solution would not be expected to be reliable. In this area, Rosner's theory predicts considerably shorter burning times. For lower oxidant level environments the burning times for each theory are nearly identical.

Rosner's solution is described below. Beginning with the differential equation

$$\rho \frac{\partial \Gamma}{\partial t} - \frac{D\rho}{r^2} \frac{\partial}{\partial r} \left(r^2 \frac{\partial \Gamma}{\partial r}\right) = 0 \quad . \tag{A.22}$$

Rosner defines the following quantities

$$\tau \equiv t \frac{D}{a^2} \tag{A.47}$$

and

$$\eta \equiv r/a \quad . \tag{A.48}$$

The boundary conditions and initial conditions are as follows:

at

$$\eta \to \infty \qquad \Gamma = 0 \tag{A.49}$$

$$\int_0^\infty 3\Gamma\eta^2 d\eta = 1 \qquad \text{(A.50)}$$

and at

$$\tau = 0 \qquad \eta \leq 1 \qquad \Gamma = 1 \qquad \text{(A.51)}$$

$$\tau = 0 \qquad \eta > 1 \qquad \Gamma = 0 \quad . \qquad \text{(A.52)}$$

The above are simply the dimensionless forms of Equations (A.23), (A.31), (A.32), and (A.33).

Rosner's solution of (A.22) with the boundary and initial conditions described above is

$$\Gamma = \frac{1}{2}\left[\operatorname{erf}\left(\frac{1+\eta}{2\tau^{1/2}}\right) + \operatorname{erf}\left(\frac{1-\eta}{2\tau^{1/2}}\right)\right] - \frac{\tau^{1/2}}{\Pi^{1/2}\eta}\left\{\exp\left[-\frac{(1-\eta)^2}{4\tau}\right] - \exp\left[-\frac{(1+\eta)^2}{4\tau}\right]\right\}. \qquad \text{(A.53)}$$

At the flame surface, from Equation (A.37)

$$\Gamma_f = \frac{Y_{0\infty}}{\frac{\nu_0 W_0}{\nu_F W_F} + Y_{0\infty}} \quad . \qquad \text{(A.37)}$$

Rosner defines the term

$$\nu \equiv \frac{Y_{0\infty}/Y_{F,\ell}}{\left(\frac{\nu_0 W_0}{\nu_F W_F}\right)} \quad . \qquad \text{(A.54)}$$

$Y_{F,\ell}$ is equal to 1.0 for this model. Substituting (A.54) into (A.37) yields

$$\Gamma_f = \frac{\nu}{1+\nu} \quad . \tag{A.55}$$

Rosner's solution for the flame location as a function of time is described by the equation

$$\frac{\nu}{1+\nu} = \frac{1}{2}\left[\operatorname{erf}\left(\frac{1+\eta_f}{2\tau^{1/2}}\right) + \operatorname{erf}\left(\frac{1+\eta_f}{2\tau^{1/2}}\right)\right]$$

$$- \frac{\tau^{1/2}}{\Pi^{1/2}\eta_f}\left\{\exp\left[-\frac{(1-\eta_f)^2}{4\tau}\right] - \exp\left[-\frac{(1+\eta_f)^2}{4\tau}\right]\right\} . \tag{A.56}$$

Reference 15 shows the dimensionless flame radius, η_f, as a function of τ, the dimensionless time, for both the Spalding and Rosner models.

The end of burning occurs when $\eta_f \to 0$. Examining Equation (A.56) it is seen that as η_f goes to zero the second term on the right hand side becomes indeterminate. The exponential terms subtract out in the numerator and η_f goes to zero in the denominator. If L'Hospital's Rule is applied to this term, the solution for the burning time satisfies the equation

$$\frac{\nu}{1+\nu} = \operatorname{erf}\left(\frac{1}{2\tau_b^{1/2}}\right) - \frac{1}{(\Pi\tau_b)^{1/2}} \exp\left(-\frac{1}{4\tau_b}\right) . \tag{A.57}$$

A comparison of the dimensionless burning times as a function of ν for both theories (14, 15) is shown in Figure 16 in Chapter 4.

To find the pressure dependence of the dimensional burning times in Rosner's solution, it must be noted that for a given value

of the stoichiometry parameter, τ_b is fixed. From the definition of τ_b, it is seen that

$$t_b = \tau_b \frac{a^2}{D} \quad . \tag{A.58}$$

Since the product (ρD) is relatively unaffected by pressure, this equation may be written

$$t_b = \tau_b \frac{a^2}{(\rho D)} \quad . \tag{A.59}$$

The apparent radius, a, is proportional to $\rho^{-1/3}$, and ρ is proportional to pressure, for the assumptions used in this analysis. Thus, the burning time is proportional to the cube root of pressure.

Since a is proportional to r_ℓ, the droplet lifetime is proportional to the initial droplet diameter squared. This result agrees with Spalding's.

APPENDIX B

ANALYSIS OF THE THERMOCOUPLE TIME RESPONSE

It was felt that an indication of the thermocouple's ability to follow the temperature of the droplet would be a comparison of the time constant of the thermocouple bead in the droplet liquid with the time constant of the spherical droplet immersed in gas. Examining a model where a spherical particle is in equilibrium with a fluid bath at T_f, and the fluid undergoes a step change in temperature, an energy balance on the particle yields

$$\frac{\rho V c_p}{hA} \frac{dT}{dt} = T_f - T \quad . \tag{B.1}$$

The time constant is the quantity

$$\tau' = \frac{\rho V_{cp}}{Ah} \quad . \tag{B.2}$$

The film coefficient is $h = NuK_f/D_p$. For a spherical particle in the absence of convection, Nu = 2.0. Also for a sphere $V/A = D_p/6$. Substituting into (B.2) yields

$$\tau' = \frac{\rho c_p D_p^2}{12K_f} \quad . \tag{B.3}$$

Table 3 shows the numerical values used in calculating the thermocouple and droplet time constants. The gas is taken to be

air with properties evaluated at 1940°F, and the droplet liquid is n-decane. The thermocouple bead is assumed to consist of 50 percent chromel and 50 percent alumel by weight. Properties were obtained from References 19, 26, 27, 28, and 29. Substituting the values from Table 3 into Equation (B.3) gives τ'_D = 1.9 sec and τ'_{tc} = 0.103 sec. Thus, the time constant for the droplet is 10.8 times that of the thermocouple bead, indicating that the thermocouple should follow the droplet temperature with no difficulty.

TABLE 3

PROPERTIES USED IN CALCULATION OF TIME CONSTANTS

	Thermocouple Bead	Liquid Droplet
ρ lb_m/ft^3	541	45.79
c_p Btw/lb_m-°F	0.116	0.588
k_f Btw/hr-ft-°F	0.081	0.053
D_p in.	0.008	0.030

APPENDIX C

ANALYSIS OF THE HEAT CONDUCTED FROM THE FLAME TO THE DROPLET BY THE THERMOCOUPLE WIRES

A simplified model was used to estimate the amount of heat transferred to the droplet from the flame by means of the thermocouple wires. This was compared to the heat conducted from the flame to the droplet through the surrounding gas. The following assumptions were made in the analysis:

1. Heat transfer was quasi-steady, i.e. $\partial/\partial t = 0$.
2. The perfect gas assumption was made with constant fluid properties.
3. Mass flow was neglected.
4. Spherical symmetry was assumed.
5. Convection on the surface to the thermocouple wires was neglected.

Employing the above assumptions, the differential energy equation for heat conducted through the surrounding gas is

$$\frac{d}{dr}\left(r^2 \frac{dT}{dr}\right) = 0 \qquad (C.1)$$

with the boundary conditions

$$r = r_\ell \quad , \quad T = T_\ell \qquad (C.2)$$

$$r = r_f \quad , \quad T = T_f \qquad (C.3)$$

solution of (C.1) with the boundary conditions yields

$$q_f = k_g A_\ell \frac{(T_f - T_\ell)}{(r_\ell - r_f)} \frac{r_f}{r_\ell} \quad . \tag{C.4}$$

Heat conduction through the thermocouple wires is essentially a one-dimensional problem since convection from the surface of the wires is neglected. The energy equation becomes

$$\frac{d^2T}{dr^2} = 0 \tag{C.5}$$

with the boundary conditions

$$r = r_\ell \quad , \quad T = T_\ell \tag{C.6}$$

$$r = r_f \quad , \quad T = T_f \quad . \tag{C.7}$$

Solution of (C.5) with (C.6) and (C.7) yields

$$q_w = k_w A_w \frac{T_f - T_\ell}{r_f - r_\ell} \quad . \tag{C.8}$$

Thus from (C.8) and (C.4)

$$\frac{q_w}{q_f} = \frac{k_w}{k_g} \frac{A_w}{A_\ell} \frac{r_\ell}{r_f} \quad . \tag{C.9}$$

The thermocouple wires were chromel and alumel, so an average thermal conductivity for the two materials was used for k_w, equal to 14.13 Btw/hr-ft-°F. The wire radius was 0.0015 in., so that A_w for the two wires was equal to 1.418×10^{-5} in^2. The droplet radius r_ℓ was equal to 0.0173 in. and r_f was 0.15 in. The surface area of the

droplet was 0.0038 in^2. The gas was taken to be air at 1700°R, so that k_g = 0.041 Btw/hr-ft-°R. The property values were taken from References 26 and 27. Substituting the above values into (C.9) yields

$$\frac{q_w}{q_f} = 14.81 \text{ percent}$$

for this highly simplified analysis.

BIBLIOGRAPHY

1. Priem, R. J., "Propellant Vaporization as a Criterion for Rocket Engine Design: Calculations of Chamber Length to Vaporize a Single n-Heptane Drop," NACA TN 3985, July, 1957.

2. Priem, R. J. and Heidmann, M. F., "Propellant Vaporization as a Design Criterion for Rocket Engine Combustion Chambers," NASA Technical Report R-67, 1960.

3. Spalding, D. B., "The Combustion of Liquid Fuels," Fourth Symposium (International) on Combustion, Williams and Wilkins, Baltimore, 1953, pp. 847-864.

4. Godsave, G. A. E., "Studies of the Combustion of Drops in a Fuel Spray--The Burning of Single Drops of Fuel," Fourth Symposium (International) on Combustion, Williams and Wilkins, Baltimore, 1953, pp. 818-830.

5. Hottel, H. C., Williams, G. C. and Simpson, H. C., "Combustion of Droplets of Heavy Liquid Fuels," Fifth Symposium (International) on Combustion, Reinhold, New York, 1954, pp. 101-129.

6. Kobayasi, K., "An Experimental Study of the Combustion of a Fuel Droplet," Fifth Symposium (International) on Combustion, Reinhold, New York, 1954, pp. 141-148.

7. Bolt, J. A. and Saad, M. A., "Combustion Rates of Freely Falling Drops in a Hot Atmosphere," Sixth Symposium (International) on Combustion, Reinhold, New York, 1956, pp. 717-725.

8. El Wakil, M. M. Uyehara, O. A. and Myers, P. S., "A Theoretical Investigation of the Heating Up Period of Injected Fuel Droplets Vaporizing in Air," NACA TN 3179, May, 1954.

9. El Wakil, M. M., Priem, R. J., Brikowski, H. J., Myers, P. S. and Uyehara, O. A., "Experimental and Calculated Temperature and Mass Histories of Vaporizing Fuel Drops," NACA TN 3490, January, 1956.

10. Borman, G. L., El Wakil, M. M., Uyehara, O. A. and Myers, P. S., Graphs of Reduced Variables for Computing Histories of Vaporizing Fuel Drops and Drop Histories Under Pressure," NACA TN 4338, September, 1958.

11. Williams, F. A., "On the Assumptions Underlying Droplet Vaporization and Combustion Theories," Journal of Chemical Physics, Volume 33, Number 1, pp. 131-144.

12. Brzustowski, T. A., "Chemical and Physical Limits on Vapor--Phase Diffusion Flames of Droplets," The Canadian Journal of Chemical Engineering, Volume 43, February, 1965, pp. 30-35.

13. Wieber, P. R., "Calculated Temperature Histories of Vaporizing Droplets to the Critical Point," AIAA Journal, Volume 1, Number 12, December, 1963, pp. 2764-2770.

14. Spalding, D. B., "Theory of Particle Combustion at High Pressures," ARS Journal, Volume 29, November 1959, pp. 828-835.

15. Rosner, D. E., "On Liquid Droplet Combustion at High Pressures," AIAA Journal, Volume 5, Number 1, January, 1967, pp. 163-166.

16. Hall, A. R. and Diederichsen, J., "An experimental Study of the Burning of Single Drops of Fuel in Air at Pressures up to Twenty Atmospheres," Fourth Symposium (International) on Combustion, Williams and Wilkins, Baltimore, 1953, pp. 837-846.

17. Brzustowski, T. A. and Natarajan, R., "Combustion of Aniline Droplets at High Pressures," Canadian Journal of Chemical Engineering, Volume 44, August, 1966, pp. 194-201.

18. Kumagai, S. and Isoda, H., "Combustion of Fuel Droplets in a Falling Chamber," Sixth Symposium (International) on Combustion, Reinhold, New York, 1956, pp. 726-731.

19. Rossini, F. D., Pitzer, K. S., Arnett, R. L., Braun, R. M. and Pimentel, G. C., Selected Values of Physical and Thermodynamic Properties of Hydrocarbons and Related Compounds, Carnegie Press, Pittsburgh, Pa., 1953.

20. Perry, J. H., Chemical Engineer's Handbook, McGraw-Hill Book Company, Inc., New York, 1950.

21. Steffensen, R. J., Agnew, J. T. and Olsen, R. A., "Tables for Adiabatic Gas Temperature and Equilibrium Composition of Six Hydrocarbons, Engineering Bulletin of Purdue University, Lafayette, Indiana, 1966.

22. Reid, R. C. and Sherwood, T. K., The Properties of Gases and Liquids, McGraw-Hill Book Company, Inc., New York, 1958.

23. Hirschfelder, J. O., Curtiss, C. F. and Bird, R. B., Molecular Theory of Gases and Liquids, John Wiley and Sons, Inc., New York, 1954.

24. Slattery, J. C., M. S. Thesis in Chemical Engineering, University of Wisconsin, 1955. Quoted by Bird, R. B., in Drew, T. B. and Hoopes, J. W., (eds.), Advances in Chemical Engineering, Volume 1, p. 156, Academic Press, Inc., New York, 1956.

25. Williams, F. A., Combustion Theory, Addison-Wesley Publishing Company, Inc., Reading, Mass., 1965.

26. Hoskins Manufacturing Company, Chromel-Alumel Thermocouple Alloys, Detroit 8, Michigan, 1961.

27. Keenan, J. H. and Kaye, J., Gas Tables, John Wiley and Sons, Inc., New York, 1948.

28. Hodgman, C. D., (ed.), Handbook of Chemistry and Physics, Chemical Rubber Publishing Company, Cleveland, Ohio, 1958.

29. Doss, M. P., Physical Constants of the Principle Hydrocarbons, The Texas Company, New York, 1943.

REPORT DISTRIBUTION LIST FOR

CONTRACT NO. NGR 39-009-077

Applied Physics Laboratory
The John Hopkins University
Attn: W. G. Berl
8621 Georgia Avenue
Silver Spring, Maryland 20910

AFRPL (RPRRC)
Attn: B. R. Bornhorst
Edwards, California 93523

Dynamics Science Corporation
Attn: B. P. Breen
1900 Walker Avenue
Monrovia, California 91016

Chemical Propulsion Information Agency
Attn: T. W. Christian
8621 Georgia Avenue
Silver Spring, Maryland 20910

Rocketdyne
A Div. of North American Aviation
Attn: E. C. Clinger
6633 Canoga Avenue
Canoga Park, California 91304

NASA
Lewis Research Center
Attn: E. W. Conrad, Mail Stop 100-1
21000 Brookpark Road
Cleveland, Ohio 44135

U. S. Naval Weapons Center
Attn: D. Couch
China Lake, California 93555

Multi-Tech., Inc.
Attn: F. B. Cramer
601 Glenoaks Blvd.
San Fernando, California 91340

Aerospace Corporation
Attn: O. W. Dykema
P. O. Box 95085
Los Angeles, California 90045

Ohio State University
Dept. of Aeronautical and
Astronautical Engineering
Attn: R. Edse
Columbus, Ohio 43210

TRW Systems
Attn: G. W. Elverum
1 Space Park
Redondo Beach, California 90278

The Pennsylvania State University
Mechanical Engineering Department
Attn: G. M. Faeth
207 Mechanical Engineering Blvd.
University Park, Pennsylvania 16802

Pratt & Whitney Aircraft
Florida Research & Development Ctr.
Attn: G. D. Garrison
P. O. Box 2691
West Palm Beach, Florida 33402

University of Southern California
Dept. of Mechanical Engineering
Attn: M. Gerstein
University Park
Los Angeles, California 90007

Princeton University
James Forrestal Campus Library
Attn: I. Glassman
P. O. Box 710
Princeton, New Jersey 08540

Defense Research Corporation
Attn: B. Gray
P. O. Box 3587
Santa Barbara, California 93105

Princeton University
James Forrestal Campus Library
Attn: D. Harrje
P. O. Box 710
Princeton, New Jersey 08540

Aerojet-General Corporation
Attn: R. J. Hefner
P. O. Box 296
Dept. 4921 Building 160
Azusa, California 91703

Office of Naval Reserach
Navy Department
Attn: R. D. Jackel, 429
Washington, D. C. 20360

Rocketdyne
A Div. of North American Aviation
Attn: R. B. Lawhead
6633 Canoga Avenue
Canoga Park, California 91304

NASA
Headquarters
Attn: R. S. Levine, Code RPL
6th & Independence Avenue, S. W.
Washington, D. C. 20546

Dartmouth University
Attn: P. D. McCormack
Hanover, New Hampshire 03755

Colorado State University
Dept.
Attn: C. E. Mitchell
Fort Collins, Colorado 80521

University of Wisconsin
Mechanical Engineering Department
Attn: P. S. Myers
1513 University Avenue
Madison, Wisconson 53705

University of Michigan
Aerospace Engineering
Attn: J. A. Nicholls
Ann Arbor, Michigan 48104

University of California
Department of Chemical Engineering
Attn: A. K. Oppenhiem
6161 Etcheverry Hall
Berkeley, California 94720

Purdue University
School of Mechanical Engineering
Attn: J. R. Osborn
Lafayette, Indiana 47907

United Technology Center
Attn: R. H. Osborn
P. O. Box 358
Sunnyvale, California 94088

U. S. Naval Weapons Center
Attn: E. W. Price, Code 508
China Lake, California 93555

NASA
Lewis Research Center
Attn: R. J. Priem, MS-7-1
21000 Brookpark Road
Cleveland, Ohio 44135

Sacramento State College
School of Engineering
Attn: F. H. Reardon
60000 J. Street
Sacramento, California 95819

NASA
George C. Marshall Space Flight Ctr.
R-P & VE-PA, Attn: R. J. Richmond
Huntsville, Alabama 35812

Jet Propulsion Laboratory
California Institute of Technology
Attn: J. H. Rupe
4800 Oak Grove Drive
Pasadena, California 91103

Thiokol Chemical Corporation
Reaction Motors Division
Attn: C. Sage
Denville, New Jersey 07834

University of California
Mechanical Engineering, Thermal Sys.
Attn: R. Sawyer
Berkeley, California 94720

ARL (ARC)
Attn: K. Scheller
Wright-Patterson AFB
Dayton, Ohio 45433

IDA
Attn: W. C. Strahle
400 Army - Navy Drive
Arlington, Virginia 22202

NASA
Manned Spacecraft Center
Attn: J. G. Thibadaux
Houston, Texas 77058

GCA Corporation
Attn: A. C. Tobey
174 Middlesex Turnpike
Burlington, Massachusetts 01803

Massachusetts Institute of Technology
Dept. of Mechanical Engineering
Attn: T. Y. Toong
Cambridge, Massachusetts 02139

Illinois Institute of Technology
RM 200 M. H.
Attn: T. P. Torda
3300 S. Federal Street
Chicago, Illinois 60616

The Warner & Swasey Company
Control Instrument Division
Attn: R. H. Tourin
32-16 Downing Street
Flushing, New York 11354

United Aircraft Corporation
Research Labs.
Attn: D. H. Utvick
400 Main Street
East Hartford, Connecticut 06108

U. S. Army Missile Command
AMSMI-RKL, Attn: W. W. Wharton
Redstone Arsenal, Alabama 35808

University of California
Aerospace Engineering Department
Attn: F. A. Williams
P. O. Box 109
LaJolla, California 92038

Air Force Office of Scientific
Research
Attn: B. T. Wolfson
1400 Wilson Blvd.
Arlington, Virginia 22209

Bell Aerosystems Company
Attn: L. M. Wood
P. O. Box 1
Mail Zone J-81
Buffalo, New York 14205

Georgia Institute of Technology
Aerospace School
Attn: B. T. Zinn
Atlanta, Georgia 30332

NASA
Lewis Reserach Center
Attn: Paul R. Wieber
Mail Stop 7-1
21000 Brookpark Road
Cleveland, Ohio 44135